# DYNAMICS OF THE $NH_3$ LASER

by

JONATHON DAVID WHITE, B. Eng.

A Thesis

Submitted to the School of Graduate Studies

in Partial Fulfilment of the Requirements

for the Degree

Doctor of Philosophy

McMaster University

1991

DOCTOR OF PHILOSOPHY (1991) McMASTER UNIVERSITY

(Engineering Physics) Hamilton, Ontario

TITLE: **Dynamics of the $NH_3$ Laser**

AUTHOR: Jonathon David White, B. Eng. (McMaster University)

SUPERVISOR: Professor J. Reid

NUMBER OF PAGES: xii, 80

# DYNAMICS OF THE $NH_3$ LASER

**Abstract**

An experimental and theoretical study of the dynamics of $NH_3$ lasers is presented. The significant achievements of this work are summarized below.

In initial experiments, a pulsed transversely-excited $CO_2$ laser operating on the 9R(30) transition is used to optically pump mixtures of $NH_3$ in buffer gas. A simple oscillator/amplifier system allows the performance of the $NH_3$ amplifier in the 11 $\mu$m region to be characterized. Small-signal gain coefficients of >10%/cm are measured on the aQ(3,3) transition at 10.8 $\mu$m, while pump conversion efficiencies of ~50% are shown to occur under saturation conditions. The $NH_3$ laser system is described by a rate-equation model, which is validated by comparison with experiment over a wide range of operating conditions. Measurements are made for $NH_3$ concentrations ranging form 0.05 to 0.2%, for Ar, $N_2$ and He buffer gas pressures from 170 to 700 Torr, and for gas temperatures from 200 to 300 K. Optically pumped $NH_3$ is shown to be a versatile and efficient system for the amplification of mid-infrared radiation.

The rate-equation model is used to aid in the design of a simple and efficient $NH_3$ laser. This laser is tuned over more than 70 vibrational band transitions between 10.08 and 14.14 $\mu$m. Output energies greater than 1 J per pulse are achieved on several of the strongest lines. In a non-selective cavity an energy conversion efficiency of greater than 35% is obtained with a maximum output energy of 4.6 J. Optically pumped $NH_3$ is shown to be a flexible and efficient system for the downconversion of $CO_2$ radiation to the 10 - 14 $\mu$m region.

In other experiments, it is shown that optically pumped high pressure mixtures of $NH_3$ in $N_2$ are efficient, broadband amplifiers of pulsed $CO_2$ radiation. In a dilute

$NH_3$ mixture at 6 atmospheres and 200 K, a single pass gain of 150 (21.8 dB) is measured for the 10P(34) $CO_2$ transition. Gain is observed in $NH_3$ at pressures as high as 10 atmospheres. Experimental measurements are made for a range of wavelengths in the 10.7 $\mu$m region, and the results compared with calculations based on a simplified rate-equation model.

The operation of a two-step optically pumped $NH_3$ laser (using two $CO_2$ lasers) is examined. Output is obtained from 16 - 22 $\mu$m. Experimental measurements made at 200 K and 300 K are compared to calculations based on an extended rate-equation model. As a result of this work it was shown that a single $CO_2$ pump laser can be used to obtain 16 - 22 $\mu$m lasing at 200 K.

**Acknowledgments**

I would sincerely like to thank my supervisor, Dr. John Reid, for his guidance and support throughout the course of this work. I especially appreciate his willingness to commute monthly from Ottawa to meet with me at McMaster.

I am also very appreciative of the assistance given to me by Dr. Doug Bruce on amplifier work, Dr. Alok Chakrabarti on $1\nu_2$ oscillator work and Pierre Dubé on $2\nu_2$ oscillator work. I would also like to thank Fran Allen for printing many pages for me on her laser printer and for signing numerous purchase orders; Dr. Dan Cassidy who made sure I worked safely; and Dr. Tom Timusk for many helpful suggestions regarding the style of my thesis.

I would also like to thank my brothers and sisters in Christ for their prayer support and my parents for their spiritual, emotional and physical support.

Finally, to God who has provided comfort, encouragement, and an opportunity to grow through these last 4½ years.

> Meaningless, meaningless, all is meaningless. What profit hath a man for all his labour which he taketh *under the sun*? One generation dies and another is born. There is no remembrance of former things.
>
> Let us hear the conclusion of the whole matter: Fear God, and keep his commandments: for this is the whole duty of man. For God shall bring every work into judgement, with every secret thing, whether it be good or whether it be evil. (from The Preacher)

## Table of Contents

## List of Figures

## List of Tables

## List of Symbols

| | |
|---|---|
| A | thermal equilibrium ratio $N_1/N_0$ (chap. 5) |
| B | thermal equilibrium ratio $N_2/N_1$ (chap. 5) |
| $B_a$ | thermal equilibrium ratio $N_2a/N_1$ (chap. 5) |
| $B_{as}$ | thermal equilibrium ratio $N_2a/N_2s$ (chap. 5) |
| $B_s$ | thermal equilibrium ratio $N_2s/N_1$ (chap. 5) |
| f | thermal equilibrium fraction $r_i/N_i$ |
| $g_i$ | degeneracy of i'th rotational level |
| $g_l$ | degeneracy of lower pumped rotational level |
| $g_u$ | degeneracy of upper pumped roational level |
| $I_p$ | pump intensity |
| $I_s$ | probe intensity |
| J | total angular momentum excluding nuclear spin |
| $k_{NH3}$ | $1\nu_2 \leftarrow$ gs VT relaxation rate for $NH_3$ - $NH_3$ collisions |
| $k_m$ | $1\nu_2 \leftarrow$ gs VT relaxation rate for $NH_3$ - buffer collisions |
| K | quantum number of component of angular momentum along molecular axis |
| K | rotational coupling parameter |
| N | total population of $NH_3$ molecules |
| $N_0$ | population of the ground vibrational state |
| $N_1$ | population of the $\nu_2 = 1$ vibrational state |
| $N_2$ | population of the $\nu_2 = 2$ vibrational state |
| P | pumping rate |

| | |
|---|---|
| $p_{NH3}$ | partial pressure of $NH_3$ |
| $p_m$ | partial pressure of buffer gas |
| $r_i$ | population of the i'th rotational level |
| $s_i$ | population of the i'th rotational level |
| $r_i^e$ | thermal equilibrium population of i'th rotational level |
| $\alpha$ | absorption coefficient |
| $\sigma$ | absorption cross section |
| $\tau_i$ | characteristic time for rotational relaxation in the i'th vibrational level (chap. 2) |
| $\tau_{10}$ | characteristic time for VT relaxation from the first vibrational level to the ground state (chap. 5) |
| $\tau_{21}$ | characteristic time for VT relaxation from the second vibrational level to the first vibrational level (chap. 5) |
| $\tau_{as}$ | characteristic time for $2\nu_2 a \leftarrow 2\nu_2 s$ conversion |
| $\tau_r$ | characteristic time for rotational relaxation (chap. 5) |
| $\tau_{VT}$ | characteristic time for VT relaxation from the first vibrational level to the ground state |
| $\tau_{VV}$ | characteristic time for VV relaxation |
| $\nu_p$ | pump frequency |
| $\nu_s$ | probe frequency |
| $\Delta\nu$ | pressure broadened HWHM of ammonia transitions |

## Chapter 1

## Introduction

Optically pumped molecular lasers (OPML's) have been widely investigated as sources of line-tunable radiation in the infrared. Pulsed transversely-excited (TE) $CO_2$ lasers are commonly used as the optical pump with the goal of developing efficient, line-tunable oscillators. Optically pumped $NH_3$ lasers have proven to be one of the most successful lasers of this type. Lasing has been observed throughout the mid-infrared from 6 to 35 $\mu$m [1] with over 50 known $NH_3$ laser lines in the 10.3 to 13.8 $\mu$m region [2,3], while measured pulsed energies of 1.5 J [4] and conversion efficiencies of 28% [5] make $NH_3$ the most powerful and efficient optically pumped mid-infrared laser. The $NH_3$ laser has been used for isotope selective dissociation of $CCl_4$ [6], $SeF_6$ [7] and for tritium/deuterium separation [8].

Excellent papers reviewing research in OPML's have been published by Gupta *et al.* [9] and Harrison [10]. These papers provide a summary of the history of research into $NH_3$ lasers up until 1986. Recent work has focused on the development of ultrastable $NH_3$ lasers [11]; the development of compact waveguide lasers with GHz tunability [12]; the observation and quantification of chaos in various $NH_3$ laser systems [13,14]; and, the development of highly efficient inversion $NH_3$ lasers. This latter area is the central focus of the work described in this thesis which has been to verify, refine and extend the rate equation approach of Morrison *et al.* [15], using the results to optimize the behaviour of $NH_3$ amplifiers and oscillators.

In chapter 2, detailed measurements of the performance of $NH_3$ amplifiers under both small-signal and saturated gain conditions are reported. The measured

gain coefficients are compared with the predictions of a rate equation model developed by Morrison [15,16,17,18]. We have validated the model by comparison with experiment results covering a wide range of amplifier pressures (170 - 700 Torr), temperatures (200 - 300 K), mixtures (0.05 - 0.2% $NH_3$) and buffer gases (Ar, $N_2$ and He). The $CO_2$ pump intensities range from 20 to 120 kW/cm$^2$. Gain measurements were made for several different $NH_3$ transitions, and agreement with the model was better than ±15% under all conditions.

Chapter 3 utilizes the model developed and verified in chapter 2 to aid in the design of a simple laser configuration offering improved performance. The experimental configuration overcomes some of the limitations of previous work which required complicated configurations in which it is often difficult to change pump or emission wavelengths. By using a dilute mixture of $NH_3$ in a few hundred Torr of argon as the active medium, pulsed lasing on the sP(10,K), aP(9,K), aP(10,K), and aP(11,K) rotational-vibrational transitions was observed for the first time, thus extending the line-tunable range of the regular $NH_3$ laser to wavelengths longer than 14 $\mu$m. In total, lasing was observed on over 70 transitions and our results represent, to the best of the writer's knowledge, the highest energy conversion efficiencies reported to date for any OPML operating in the mid-infrared [9,10].

In chapter 4 the operation of ammonia amplifiers at high pressure is examined. A set of rate equations to model the $NH_3$ system is developed, and the model verified by experimental measurements at a number of frequencies, pressures, concentrations and temperatures. Experimentally, single pass gains of 150 (21.8 dB) are observed in dilute $NH_3$ mixtures at 6 atmospheres for the 10P(34) $CO_2$ transition. At this pressure the gain bandwidth in $NH_3$ is ~4 cm$^{-1}$, suitable for amplifying pulses as short as a few picoseconds.

Chapter 5 records the results of an experimental and theoretical investigation into the feasibility of building efficient hot-band ammonia lasers. Experimental measurements were taken at both 200 K and 300 K. Results at 300 K indicate performance in accord with the predictions of the model, while results at 200 K are somewhat surprising as they indicate better performance than that predicted by the model.

Chapter 6 summarizes the work discussed in this thesis and makes suggestions on the direction of future research.

# Chapter 2

## Amplifier Theory and Experiments

### 2.0 Introduction

Optically pumped $NH_3$ lasers have been widely investigated as sources of line-tunable radiation in the 10 to 13 $\mu$m region; however, only limited investigations have been carried out to characterize the behaviour of optically pumped $NH_3$ as an amplifier [16,17,19].

The main thrusts of the experiments described in this chapter were to verify the small signal inversion gain model of Morrison *et al.* [17]; extend it to the case of saturated gain; and, to demonstrate that $NH_3$ amplifiers are highly efficient converters of $CO_2$ radiation giving significant gain in the 10.8 $\mu$m region. Gain coefficients were measured ranging from 5 to 15%/cm on the aQ(3,3) transition at 927 $cm^{-1}$. A power conversion efficiency from the pump beam of 46% was obtained.

The next section explains the rate equation model used to describe the dynamics of the optically pumped $NH_3$ system. The experimental apparatus and results are described in Sections 2.2 - 2.4, while a discussion and conclusions are presented in Section 2.5.

### 2.1 Theory

While several different $CO_2$ transitions have been used to optically pump $NH_3$, the most effective for line-tunable operation is the 9R(30) $CO_2$ transition at 1084.629 $cm^{-1}$. The linecentre of the 9R(30) $CO_2$ transition lies 184 MHz from the sR(5,0)

linecentre of $NH_3$*, but is also in close coincidence to additional lines in the sR(5,K) multiplet. The upper trace in Fig. 2.1 illustrates the spectroscopy in the 1084.6 $cm^{-1}$ region. The pumping and collisional transfer processes relevant to laser operation are indicated schematically in the middle diagram, while the lower portion of Fig. 2.1 shows the relative gain coefficients for the stronger $\nu_2$ transitions under typical pumping conditions.

To produce line-tunable amplification in the mid-infrared, it is first necessary to transfer population from the ground level ($\nu_2$=0) to the $\nu_2$=1 vibrational level of $NH_3$. This transfer is accomplished by pumping the sR(5,K) multiplet with resonant laser radiation. A mechanism is also required to distribute the population from the pumped rotational states in the upper vibrational level to the companion rotational states, and to repopulate the lower pumped state. This redistribution is achieved by diluting the $NH_3$ in a buffer gas such as Ar or $N_2$. Typically, $NH_3$ makes up less than 1% of the gas mixture, and collisions between the $NH_3$ and the buffer gas produce rapid rotational relaxation in both upper and lower vibrational levels. By pumping on an R-branch transition, inversion can potentially be created on all Q and P-branch transitions [25]. As both the pump and lasing transitions occur in the strong, fundamental $\nu_2$ vibrational mode of $NH_3$, very efficient operation is expected [9].

A rate-equation model has been developed to describe the dynamics of population inversion in optically pumped $NH_3$ lasers. The model evaluates changes in populations based on two main assumptions: (1) the rotational populations are always thermalized, except for the levels of the pumped transition, and (2) the ortho-species of $NH_3$ (angular momentum quantum number K = 3n), and the para-species

---

* Full descriptions of the spectroscopy of ammonia can be found in Townes and Schalow's Microwave Spectroscopy [20] and Herzberg's Infrared and Raman Spectra [21]. Excellent and equivalent descriptions of the nomenclature directly applicable to $NH_3$ oscillators and amplifiers comprise the second chapters of the theses of Morrison [15], Rolland [22,23] and Dubé [24].

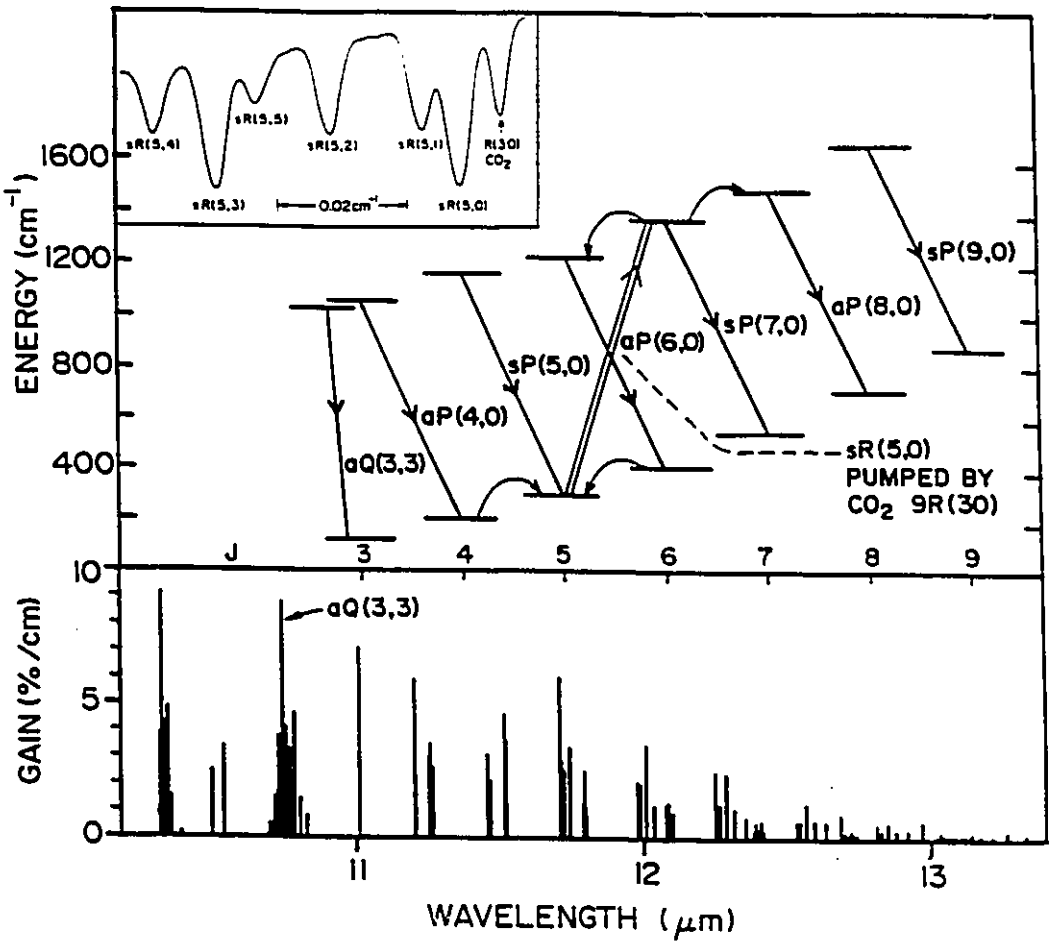


Figure 2.1: Spectroscopy and energy levels of $NH_3$ relevant to laser operation. The upper trace is a tunable diode laser scan of $NH_3$ and $CO_2$ near 1084.6 $cm^{-1}$, showing the proximity of the $CO_2$ 9R(30) line to the sR(5,0) and sR(5,1) transitions in $NH_3$ (frequency offsets of 184 and 356 MHz, respectively). The middle section is an energy level diagram of $NH_3$ showing several transitions that have gain when the sR(5,0) transition is pumped. For simplicity mostly K=0 levels are shown. The curved arrows represent the collisional processes that thermalize the population in the upper and lower levels. The lowest portion of the figure shows a gain spectrum attained under typical pumping conditions

($K = 3n \pm 1$) can be treated as two independent species. Assumption (1) is justified as the rotational rate in dilute $NH_3$ mixtures is much faster than the vibrational-translational (V-T) relaxation rate [18], and the population distribution remains close to thermal equilibrium in those levels not directly coupled to the pump radiation. Assumption (2) has been shown to be a very good approximation in experiments in which only a single species of $NH_3$ was optically pumped [2, 18], and recent direct measurements of collisional relaxation rates have shown that the rate of vibrational energy transfer between ortho- and para-$NH_3$ is very slow [26].

A computer model has been used successfully to calculate the gain in both continuous (cw) and pulsed $NH_3$ systems [15,16,17,18]. As the pump and probe pulses employed in the present series of experiments have a much longer time duration than the characteristic V-T relaxation time of the $NH_3$ gas mixtures, one can treat the laser system in a quasi-cw fashion. Therefore, the cw treatment described in detail in Ref. [18] was followed with a few minor modifications to account for the much higher gas pressures used in the present work, and to include the results of more recent measurements of relaxation rates in $NH_3$. In the model the total $NH_3$ population is assumed to lie in the ground, first and second excited states of the $\nu_2$ mode.

These vibrational levels are treated as harmonic with a fundamental frequency $\nu = 950\ cm^{-1}$, but the inversion splitting of 36 $cm^{-1}$ in the $\nu_2 = 1$ state is treated explicitly to ensure that saturation of the sR(5,0) transition is calculated accurately. All the pump and emission transitions of interest in this paper occur between the $\nu_2 = 0$ and $\nu_2 = 1$ levels. Thus the equations are written chiefly in terms of $N_0$ and $N_1$, the populations of the two lower vibrational levels. The total population N is the sum of $N_0$, $N_1$, and $N_2$, where $N_2$ is the population of the second excited state. The complete rate equations for $N_0$ and $N_1$ and the two rotational levels of the pumped transitions are given on the next page:

$$\frac{dN_0}{dt} = \frac{N_1 - x_v N_0}{\tau_{VT}} + \frac{2(N_1^2 - N_0 N_2)}{N \times \tau_{VV}} - W_p \Delta r$$

$$\equiv +P_0 - W_p \Delta r \qquad (2.1)$$

$$\frac{dN_1}{dt} = \frac{2N_2 - (1+2x_v)N_1 + x_v N_0}{\tau_{VT}} - \frac{4(N_1^2 - N_0 N_2)}{N \times \tau_{VV}} + W_p \Delta r$$

$$\equiv -P_1 + W_p \Delta r \qquad (2.2)$$

$$\frac{dr_0}{dt} = -\frac{(r_0 - r_0^e)}{\tau_0} - W_p \Delta r + P_0 \left(\frac{r_0}{N_0}\right) \qquad (2.3)$$

$$\frac{dr_1}{dt} = -\frac{(r_1 - r_1^e)}{\tau_1} + W_p \Delta r - P_1 \left(\frac{r_1}{N_1}\right) \qquad (2.4)$$

and

$$N = N_0 + N_1 + N_2$$

$$x_v = \exp\left(-\frac{h\nu}{k_B T}\right)$$

The pumping rate from rotational level $r_0$ in $N_0$ to rotational level $r_1$ in $N_1$ is

$$W_p \Delta r = \left(\frac{I_p}{h\nu_p}\right)\sigma\left[r_0 - r_1\left(\frac{g_0}{g_1}\right)\right] \tag{2.5}$$

where $I_p$ is the pump intensity at the frequency $\nu_p$, $\sigma$ is the absorption cross section, and $g_0$ and $g_1$ are the degeneracies of $r_0$ and $r_1$. The absorption cross section is calculated under the assumption that all the 9R(30) pump radiation is centred at a 184 MHz frequency offset from the sR(5,0) transition. At thermal equilibrium, with no pump present, $r_i^e = f_i N_i$. With the presence of the pump ($r_i$ is counted in $N_i$),

$$r_i^e = f_i \frac{(N_i - r_i)}{(1 - f_i)} \tag{2.6}$$

Throughout this thesis $r_0$ is the s(5,0) level in the ground state, while $r_1$ is the a(6,0) level in the $v_2 = 1$ vibrational state.

The values of the relaxation rates in the model are obtained in the following manner. The VT relaxation rate $\tau_{VT}^{-1}$ is given by [26,27,28]:

$$\tau_{VT}^{-1} = \left(k_{NH_3} p_{NH_3} + k_m p_m\right) \tag{2.7}$$

where the k's are rates and the p's are pressures of $NH_3$ and a buffer gas M. The value of $k_{NH3}$ and $k_{N2}$ are taken from Ref [26], while $k_{Ar}$ and $k_{He}$ are taken from the

work of Hovis and Moore [27,28]. Recent experimental work has shown that the vibrational-vibrational rate, $\tau_{VV}^{-1}$, is insignificant under typical $NH_3$ laser conditions, and that the population $N_2$ is simply given by [24]:

$$N_2 = x_v N_1 \tag{2.8}$$

Thus $N_2$ is always $\leq 1\%$ of $N_1$ for gas temperatures in the range 200 to 300 K. Within the accuracy of the present model, the population in $N_2$ can be ignored, and the same result in the computer simulation is achieved by making $\tau_{VV}$ very long compared with all other relaxation rates. In previous work it has been assumed that the rotational rates $\tau_o^{-1}$ and $\tau_1^{-1}$ are defined by the pressure broadened halfwidth at half-maximum of the absorption line $\Delta\nu$ given by [18]:

$$\Delta\nu = \left(\frac{\Delta\nu}{p}\right)_{NH_3} p_{NH_3} + \left(\frac{\Delta\nu}{p}\right)_m p_m \tag{2.9}$$

$$= \frac{1}{4\pi}\left(\frac{1}{\tau_0} + \frac{1}{\tau_1}\right)$$

This formula gives reasonable agreement with experimental measurements of small-signal gain, although there is some uncertainty in the value of the ratio $y = \tau_o/\tau_1$. However, as described in Section 2.5, measurements of saturated gain coefficients demonstrate that Eq. (2.9) overestimates the rate of rotational population transfer. Thus the introduction of a variable parameter, K, such that

$$K\Delta\nu = \frac{1}{4\pi}\left(\frac{1}{\tau_0} + \frac{1}{\tau_1}\right) \tag{2.10}$$

where K < 1. K is adjusted to give a best fit to the experimental results.

For the case of quasi-cw pumping, when the pump intensity $I_p$ varies slowly on the timescale of $\tau_{VT}$, the rate equations are solved for the final populations by setting all the time derivatives equal to zero. The solution is not analytic because the equations are nonlinear; hence, a numerical root finding computer program is employed to solve for $N_0$, $N_1$ and $N_2$. The final step in the model is the evaluation of the gain spectrum from the vibrational populations under the assumption of rotational thermalization. Rather than use the values of $N_1$ and $N_0$ directly, two parameters are defined that express the degree of vibrational inversion, $N_1/N_0$, and the fractional population in the ground and $\nu_2 = 1$ states, $(N_0 + N_1)/N$. The value of $N_1/N_0$ specifies the gain distribution, whereas $(N_0 + N_1)/N$ gives the fraction of the total $NH_3$ molecules which remain in the upper and lower laser levels. (As V-V transfer into the $\nu_2 = 2$ level is slow [24], $(N_0 + N_1)/N$ is typically $\geq 0.99$). A separate subroutine takes specific values of these two parameters together with, (1) the $NH_3$ partial pressure; (2) the total pressure broadening due to the buffer gas; and, (3) the rotational temperature to evaluate the gain on the $NH_3$ transitions of interest. This gain calculation includes the effect of the inversion splitting of all the vibrational states into symmetric (s) and antisymmetric (a) levels. The splitting is negligible in the ground state (0.8 $cm^{-1}$). However, in the $\nu_2 = 1$ state the splitting is 36 $cm^{-1}$ which leads to the prediction of significantly higher gain coefficients for the a-transitions than for the corresponding s-transitions.

In many of the experiments described in this chapter, the intensities of both the pump and probe beams vary significantly along the length of the amplifier. Thus a "point model" which deals with fixed intensities is not appropriate. The computer model is designed to treat an amplifier cell as many short sections, and to automatically handle the changes in intensity as the beams propagate. While the ortho

and para species of $NH_3$ are treated separately in the calculation, pump depletion due to absorption by *all* the transitions in the sR(5,K) multiplet is taken into account.

## 2.2 Experimental Technique

### *A. Apparatus*

Figure 2.2 is a schematic diagram of the apparatus. A simple oscillator/amplifier configuration is used to measure gain coefficients in the optically pumped medium. A single TE $CO_2$ laser pumps both the oscillator and the amplifier. The TE laser is a Lumonics K-902 with a discharge volume of 88 x 3.5 x 3.3 cm. operating at ~100 torr with a 8% $CO_2$:13%$N_2$:79%He mixture. This low pressure ensures that the frequency bandwidth of the $CO_2$ radiation is relatively narrow, and that the pulsed output has a long duration. When tuned to the 9R(30) transition, the laser gives an output pulse ~40 $\mu$s long with a total energy of 2.5 J.

The $CO_2$ laser pulse is split into two beams; 36% of the pulse pumps the oscillator, while the remaining pulse energy is directed into the amplifier. The $NH_3$ oscillator contains an 1 m long pyrex tube sealed with KCl Brewster windows and cooled with dry ice. Typically, the pyrex tube is filled with 0.05% $NH_3$ in Ar at a total pressure of 50 to 140 Torr. This tube operates sealed off, and one gas mixture lasts for many months. The $NH_3$ laser cavity is formed by a 60% reflecting mirror and a 135 lines/mm grating. For the gain saturation measurements, the conditions in the $NH_3$ oscillator were carefully optimised to produce aQ(3,3) $NH_3$ pulses with high energy and maximum peak power.

The probe from the oscillator and the second 9 $\mu$m pump beam are combined at a dichroic mirror before passing through the amplifier. Care was taken to optimise the transmission of both pump and probe pulses through the system. Typically, 0.8 J of pump radiation and 75 mJ of aQ(3,3) probe radiation are incident upon the

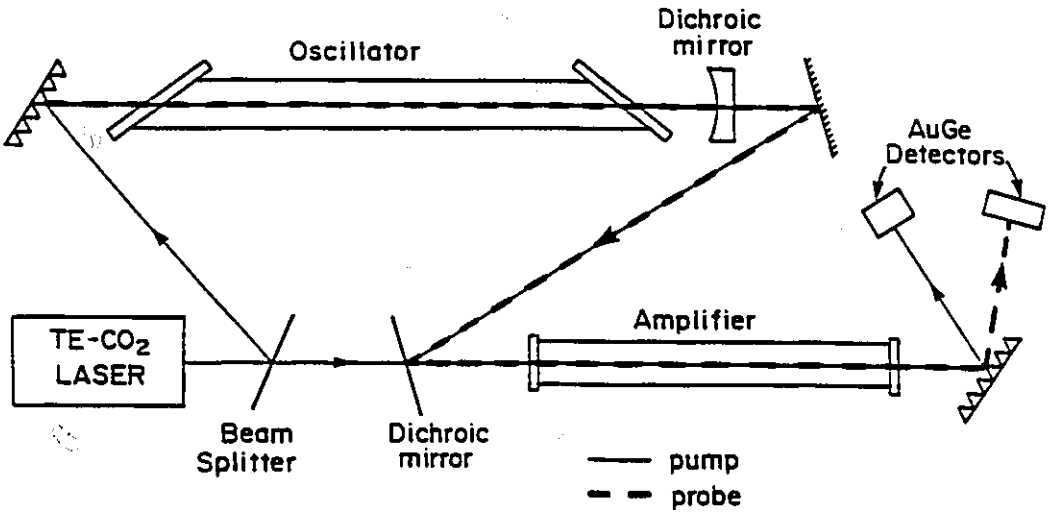


Figure 2.2: Schematic diagram of the apparatus for measuring gain in optically pumped $NH_3$

entrance window of the amplifier. When the amplifier cell is empty, these pulses result in peak powers of ~110 kW/cm$^2$ (pump) and ~15 kW/cm$^2$ (probe) exiting the cell. For the small-signal gain measurements, the $NH_3$ oscillator was operated at lower pressures, and a series of attenuators were used to ensure that the peak pulse power was $\ll$1 kW/cm$^2$. Two amplifier tubes were used in the present study; one was 60 cm long while the other was 120 cm long. Each tube was sealed with AR-coated ZnSe windows, could be cooled with dry ice, and was generally operated with a slowly flowing gas mixture. The 6.8 mm diameter tubes act as waveguides for both the pump and probe beams. The waveguide ensures that the pump beam is confined over the length of the cell, and that the pump and probe beams have a good spatial overlap. A second grating separates the pump and probe beam after passage through the amplifier; each pulse is detected by separate Au-Ge detectors. The detector signals are then recorded on a Tektronix 468 digital oscilloscope.

*B. Measurement Technique*

Figure 2.3 displays the three pulse shapes recorded by the oscilloscope during the measurements of small-signal gain. The probe pulses are recorded both with and without $NH_3$ gas in the 60 cm amplifier, and under small-signal gain conditions we measure peak amplifications in the range of 50 to 100 per pass. During the period of this study, both the pump and probe pulses were stable and reproducible. Typically, the peak powers varied by ±3% from shot-to-shot, and long term drifts during the course of an experiment were less than ±5%. The lasers were generally operated at a repetition rate of 1 Hz, and in all cases 8 successive pulses were averaged by the oscilloscope before the data was transferred to a computer. The computer was used to calculate gain coefficients as a function of pump intensity, and to compare experiments with the predictions of the model.

To make accurate comparisons with the rate equation model, it is important that experimental parameters such as intensity and gas mixture be accurately known. We measure intensity by determining the energy of the laser pulses exiting the waveguide with a Gen-Tec ED-500 Joule meter, and scaling to the integrated area of the pulse as determined by the computer. We then divide by the area of the waveguide to determine the *average* intensity across the bore of the amplifier. In an empty waveguide, the pump and probe attenuation is small (< 10%/pass), and does not affect the model comparisons. However, there is a significant variation in the radial intensity distribution across the circular bore of amplifier. For both the pump and the probe, the measured intensity distribution corresponds closely to an $EH_{11}$ waveguide mode. This radial intensity distribution is ignored in the model calculations, as discussed in Sections 2.4 and 2.5.

If a reliable comparison is to be made between theory and experiment, it is essential that the concentration of the gas mixture be accurately known. As $NH_3$ is

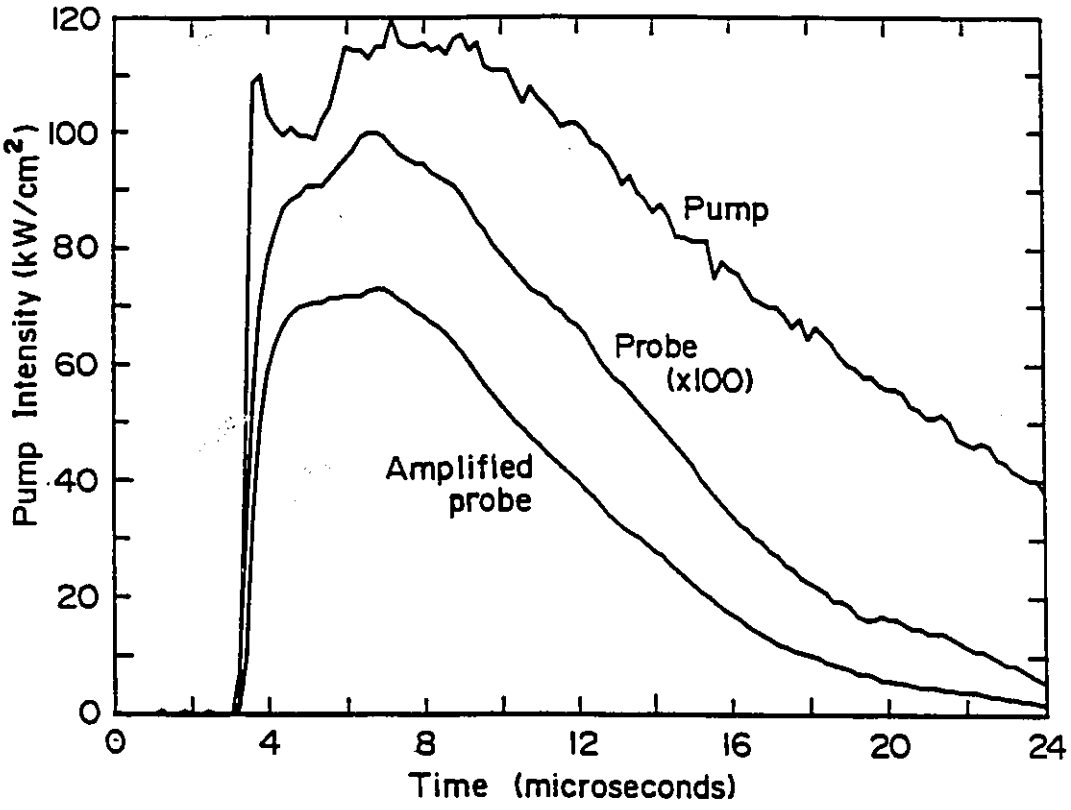


Figure 2.3: Typical pulse shapes as recorded by the digital oscilloscope. In each case, eight successive pulses are averaged to produce the plots. The 9R(30) $CO_2$ pulse pumps a mixture of 0.1% $NH_3$ in Ar at a total pressure of 170 Torr and a temperature of 200 K. The aQ(3,3) probe pulse is amplified by a factor of ~60 in the 60 cm amplifier tube (The two probe signals are displayed with arbitrary intensity units)

a reactive gas, and tends to be both absorbed and desorbed from the walls of a cell, some care must be taken in determining the gas concentration. A variety of techniques were employed to ensure that the $NH_3$ concentration present within the amplifier cell is known to ±10%. The measurements presented in this paper were all made with gas mixtures flowing slowly through the amplifier tube. A gas cylinder containing ~1% $NH_3$ in Ar was purchased from Canadian Liquid Air. The manufacturer's measured concentration was 0.745% $NH_3$ in Ar. An independent check was made on the cylinder concentration using an infrared absorption cell and

a 12 $\mu$m tunable diode laser [29]. This measured concentration was 0.75% ± 0.03%. the gas from the cylinder was further diluted with Ar using calibrated flowmeters. It is estimated that the resultant gas concentration was accurate to better than ±10%. A final check on gas concentration was made by measuring the probe absorption in a 10 cm, flowing gas cell. The gas flowing through the cell was identical to that flowing through the amplifier. It is an easy matter to convert the small-signal absorption, as measured on the aQ(3,3) transition, into an $NH_3$ concentration [29]. In all cases, the measured absorption on aQ(3,3) agreed with that predicted from the flowmeter settings to better than ±10%.

### 2.3 Results of Small-signal Gain Measurements*

The 60 cm amplifier cell was used for the small-signal gain measurements. Care was taken to ensure that the detector response was linear, and that measurements were made in the small-signal regime. Figure 2.4 is typical of the data obtained from the small-signal gain measurements. The experimental results are evaluated by calculating gain coefficients as a function of time, and then plotting the gain coefficient as a function of the pump intensity at that time. In this fashion, the three pulses shown in Fig. 2.3 can be converted into a complete record of gain coefficient versus pump intensity. As a check on experimental consistency, the pump pulse was attenuated by known factors to record the data of Fig. 2.4. Note that the measured gain coefficient at 30 kW/cm$^2$ pump intensity, for example, is relatively insensitive to whether it is measured near the peak of a weak pump pulse or in the tail of the unattenuated pump pulse. This type of measurement also confirms that gas heating has little effect on the gain coefficients at 170 Torr.

---

* Many of the initial small signal gain measurements were made by Dr. Doug Bruce at McMaster with the assistance of Paul Beckwith. However, all of the results displayed in the figures presented were recorded by J. White

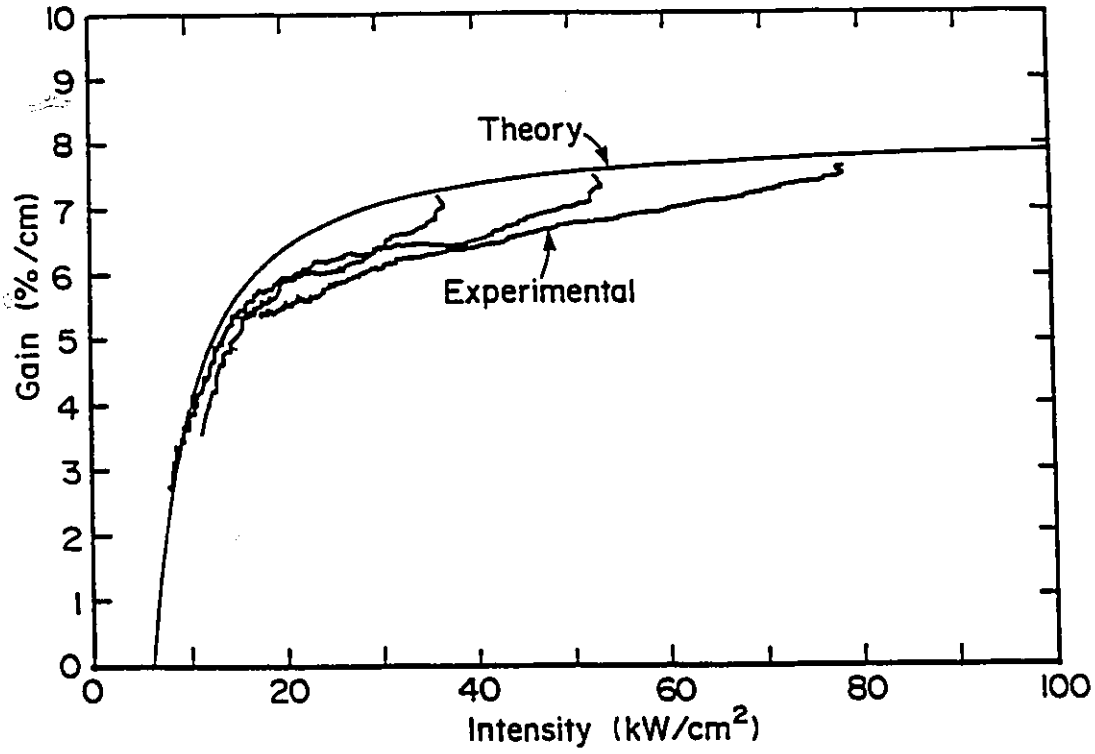


Figure 2.4: Measured and calculated small-signal gain coefficients on the aQ(3,3) transition for a 0.094% $NH_3$ in Ar mixture at 170 Torr and 200 K. The pump pulse was progressively attenuated (×0.68 and ×0.47) to produce the three experimental traces. The calculations are performed with the rotational coupling parameter, K, set equal to 0.55 (see text)

From Fig. 2.4, it can be observed that the experimental and calculated gain coefficients are insensitive to pump intensity at high intensities. The high pump intensity strongly saturates the absorption on the sR(5,0) transition, and the population inversion on aQ(3,3) is no longer dependent upon the exact value of the pump intensity, provided saturation is maintained. Under these conditions, the measured gain coefficients are independent of the exact pump distribution in the amplifier cell, both longitudinally and radially. Hence, this situation is an ideal one for a careful comparison of theory and experiment. The 170 Torr, 0.1% $NH_3$ mixture at 200 K was

treated as a standard, and gain coefficients have been measured many times over a one month period. In each case, the probe absorption was also measured in the 10 cm room temperature cell to determine the exact gas mixture. Results are summarized in Table 2.1. The important parameter in this table is the ratio of gain/absorption, as this factor is independent of minor variations of gas concentration. The reproducibility of this factor indicates the overall reproducibility of the experiment. From day-to-day, the measured value of the ratio gain/absorption varies by a maximum of ± 10%. Much of this variation is caused by variations in the pump intensity and minor changes in the relative alignment of the pump and probe beams through the amplifier. Table 2.1 also highlights the importance of maintaining a constant $NH_3$ concentration to obtain reproducible results. In general, a specific measurement of an individual gain coefficient at the peak of the pump pulse can be reproduced to better than ± 15% on a day-to-day basis. On a short term basis (~ one hour) pulse-to-pulse variations limit the reproducibility of a given measurement to ± 5%.

In Table 2.1, the experimental results are compared with two different calculations using K=1, and K=0.55. If K is set equal to 1.0, then the model assumes that all pressure broadening collisions which contribute to the linewidth also transfer rotational population from the pumped to the unpumped levels, i.e., $\tau_o$ and $\tau_1$ have the minimum possible value. Consequently, collisional transfer from the upper pumped level, a(6,0) of $\nu_2$ = 1, is most effective, and the gain on aQ(3,3) is maximised. In the next section it will be shown that K = 0.55 gives the best fit to the gain saturation data, and with this value in the model, small-signal gain is reduced by approximately 5%. The experimental measurements of small-signal gain are not accurate enough to distinguish between the two values of K, but the overall agreement between experiment and calculation is satisfactory.

TABLE 2.1: Comparison of results obtained for a nominal 0.1% $NH_3$ in Ar mixture at 170 Torr and 200 K. Pump intensity is ~75 kW/cm$^2$.

| Date of Measurement | Measured Gain Coefficient on aQ(3,3) [%/cm] | Measured Absorption Coefficient in 10 cm room temperature cell [%/cm] | Ratio [a] |
|---|---|---|---|
| June 20, 1984 | 6.6 | 9.5 | 0.70 |
| June 19, 1984 | 6.7 | 9.7 | 0.69 |
| June 18, 1984 | 5.7 | 7.0 | 0.81 |
| June 12, 1984 | 6.1 | 9.0 | 0.68 |
| June 11, 1984 | 7.8 | 12.0 | 0.65 |
| May 20, 1984 | 6.1 | 8.8 | 0.70 |

[a] Theory predicts a ratio of 0.83 (K=1) and 0.79 (K=0.55)

Theory and experiment have been compared over a wide range of amplifier conditions. Figure 2.5 shows results obtained at 360 Torr, while Table 2.2 lists results obtained for ~80 kW/cm$^2$ pump intensity. Note that Table 2.2 includes measurements made with a second probe transition, with He as a buffer gas, and at both 200 K and at room temperature. The good agreement demonstrated in Table 2.2 between theory and experiment provides confidence that the model can be reliably used to calculate small-signal gain coefficients over a wide range of amplifier conditions.

## 2.4 Results of Gain Saturation Measurements

The small-signal gain measurements described in the previous section were encouraging - large gain coefficients can be created by optical pumping, and the model enables accurate predictions to be made for a wide range of operating conditions. However, in many practical applications the $NH_3$ amplifiers will operate not in the small-signal regime, but in the saturated regime. The measurements

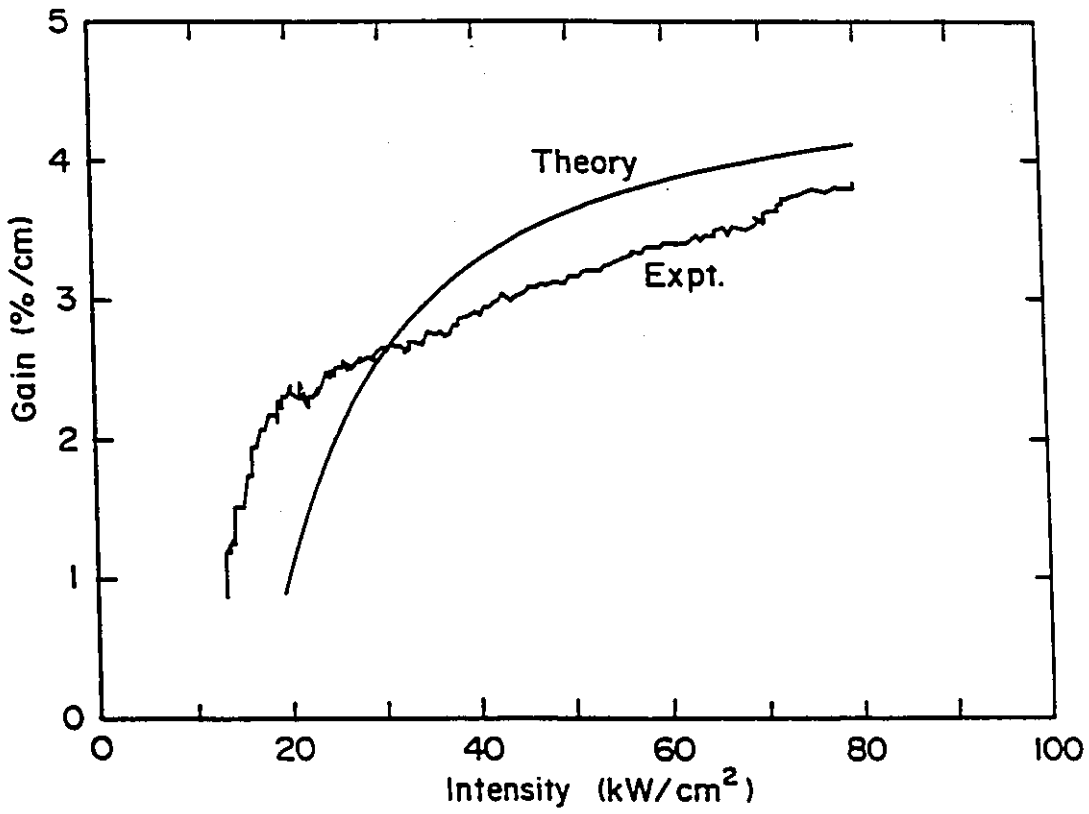


Figure 2.5: Repeat of Fig. 2.4 for a 0.053% $NH_3$ in Ar mixture at 360 Torr and 200 K. Data is recorded for the full intensity pump pulse only

described in this section were designed to evaluate amplifier performance when the probe laser power was increased to ~10 kW/cm$^2$.

The majority of the saturation measurements were made on an amplifier cell which was 120 cm long. This length allowed efficient conversion of the 9R(30) pump beam into aQ(3,3) probe radiation. Figures 2.6 and 2.7 are typical of the data recorded in the 120 cm cell. The sectioned cell model can be used to predict the amplifier performance for the conditions of Figs. 2.6 and 2.7. The model predictions, calculated by splitting the amplifier into 800 sections, are given for three values of K. Note that the calculated attenuation of the pump pulse in the absence of the probe

Table 2.2: Results of small-signal gain measurements made over a wide range of conditions.

| Conditions of Measurements | Gain Coefficient [%/cm] | |
|---|---|---|
| | Experiment [a] | Theory [K=0.55] |
| Probe operating on sP(3,0) 0.11% $NH_3$ in Ar at 170 Torr and 200 K; 80 kW/cm$^2$ pump | 4.7 | 5.0 - 5.2 [b] |
| Probe operating on sP(3,0) 0.11% $NH_3$ in Ar at 360 Torr and 200 K; 80 kW/cm$^2$ pump | 4.2 | 4.5 - 5.2 [b] |
| Probe operating on aQ(3,3) 0.23% $NH_3$ in $N_2$ at 55 Torr and 200 K; 80 kW/cm$^2$ pump | 6.6 | 7.6 |
| Probe operating on aQ(3,3) 0.23% $NH_3$ in $N_2$ at 140 Torr and 200 K; 75 kW/cm$^2$ pump | 5.9 | 6.5 |
| Probe operating on aQ(3,3) 0.058% $NH_3$ in He at 280 Torr and 200 K; 75 kW/cm$^2$ pump | 5.8 | 5.8 |
| Probe operating on aQ(3,3) 0.054% $NH_3$ in Ar at 480 Torr and 200 K; 75 kW/cm$^2$ pump | 3.6 | 3.7 |
| Probe operating on aQ(3,3) 0.093% $NH_3$ in Ar at 170 Torr and 300 K; 80 kW/cm$^2$ pump | 2.5 | 2.8 |
| Probe operating on aQ(3,3) 0.095% $NH_3$ in Ar at 360 Torr and 300 K; 80 kW/cm$^2$ pump | 2.1 | 2.4 |
| Probe operating on aQ(3,3) 0.053% $NH_3$ in Ar at 170 Torr and 200 K; 80 kW/cm$^2$ pump | 4.0 | 4.1 |

[a] The day-to-day reproduicbility of the experimental measurements is typically ± 15%

[b] Exact value of gain depends upon degree of overlap with nearby sP(3,1)

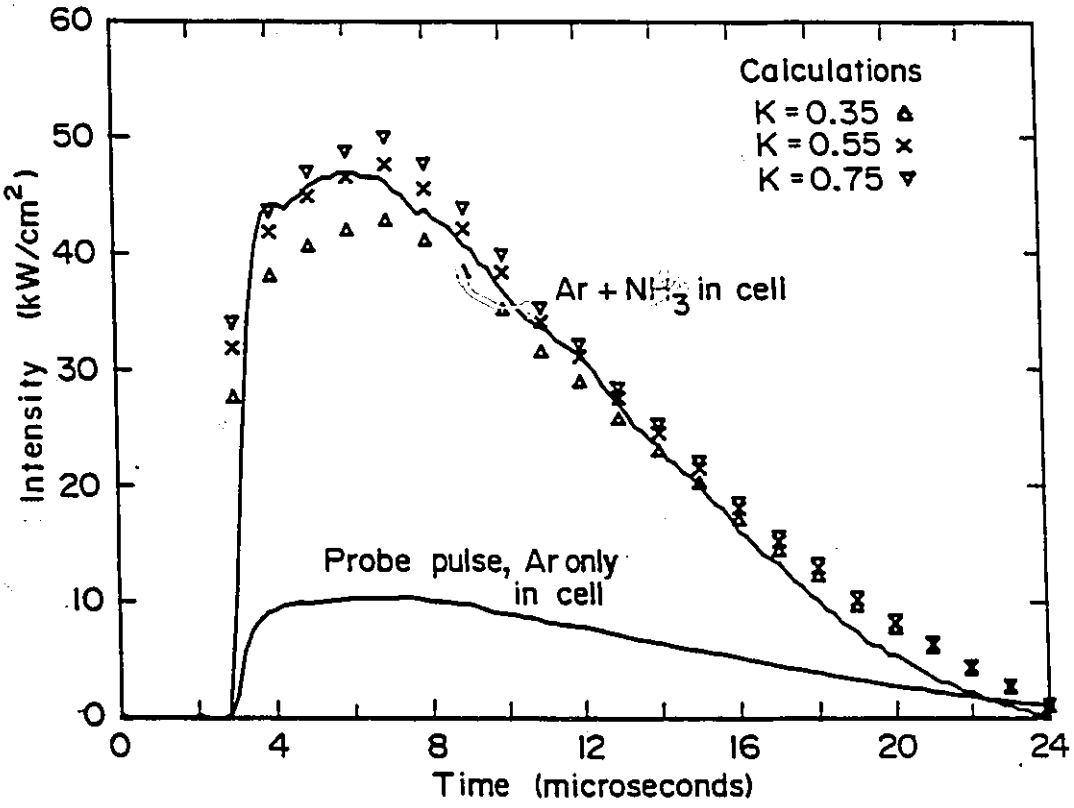


Figure 2.6: Amplification of an intense aQ(3,3) probe pulse in the 120 cm amplifier cell. Gas mixture is 0.09% $NH_3$ in 360 Torr Ar at 200 K. The theoretical points are calculated with K=0.35, 0.55 and 0.75

beam does not vary with K*. Hence the good agreement between theory and experiment confirms that the $NH_3$ concentration is correct. In a sense, a measurement of pump transmission in the absence of the probe beam is equivalent to an *in situ* measurement of $NH_3$ concentration.

*In the absence of the probe field, the pump radiation must only maintain the $\nu_2 = 1$ vibrational population against collisional relaxation via V-T transfer. As the total population in the $\nu_2 = 1$ level is insensitive to the details of rotational transfer within the level, the pump absorption does not depend upon K.

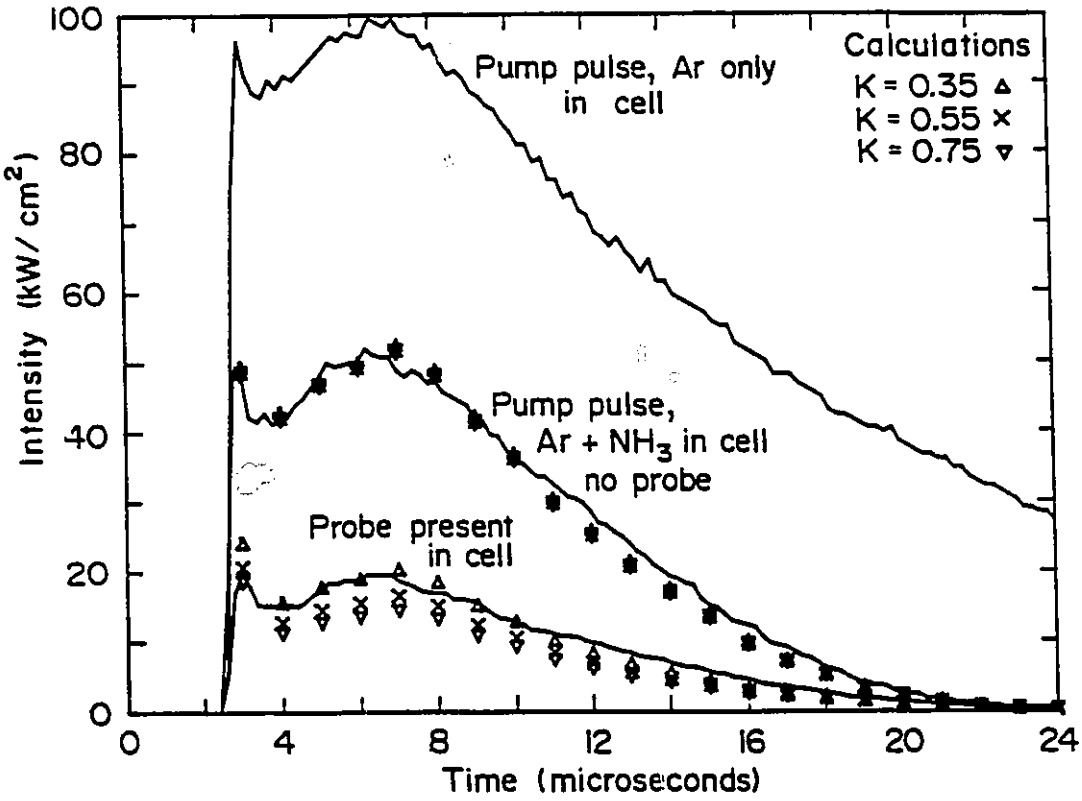


Figure 2.7: Attenuation of the 9R(30) pump pulse under the conditions given in Fig. 2.6. Theoretical points are calculated with K = 0.35, 0.55, and 0.75

When a strong probe beam is present in the amplifier, several equations must be added to the model to account for gain saturation. These equations,

$$\frac{ds_0}{dt} = -\frac{(s_0 - s_0^e)}{\tau_0} - W_s \Delta s + P_0\left(\frac{s_0}{N_0}\right) \qquad (2.11)$$

$$\frac{ds_1}{dt} = -\frac{(s_1 - s_1^e)}{\tau_1} + W_s \Delta s - P_1\left(\frac{s_1}{N_1}\right) \qquad (2.12)$$

account for the change in the populations of the lower, $s_0$, and upper, $s_1$, probed levels due to the stimulated emission term:

$$W_s \Delta S = \left(\frac{I_s}{h\nu_s}\right)\sigma_s\left[s_0 - s_1\left(\frac{g_{s0}}{g_{s1}}\right)\right] \qquad (2.13)$$

$I_s$ is the probe intensity at the frequency $\nu_s$ and the other terms are defined as in (2.5).

When the set of equations (2.1) through (2.13) are solved for quasi-cw intensities, the behaviour of the amplifier under saturation conditions is found to depend somewhat upon the value of K. For example, the efficiency with which the aQ(3,3) probe can convert photons from the 9R(30) pump depends strongly upon the rate of transfer of population from the a(6,0) level to the s(3,3) level in the $\nu_2 = 1$ vibrational level in $NH_3$. Figures 2.6 and 2.7 clearly indicate the reduction in conversion efficiency as K is changed from 0.75 to 0.35.

The type of measurements shown in Figs. 2.6 and 2.7 have been repeated for a range of operating conditions, and K used as a variable to obtain the best fit between theory and experiment. In general, all experimental results can be modelled with values of K ranging from 0.35 to 0.75. The apparent variation in K is interpreted as resulting from the minor experimental irreproducibilities (discussed on page 18). When all the experimental results are taken into consideration, as made over a wide range of mixtures, pressures and temperatures, the optimum value of K appears to be 0.55. Hence, all calculations made in the rest of this paper are carried out with K = 0.55. Figures 2.8 and 2.9 compare theory and experiment for a 120 cm amplifier cell operating at 170 Torr. Once again there is good agreement at the peak of the pump pulse confirming that the model is valid for a wide range of pump intensities. A similar agreement has been obtained for $NH_3$ concentrations ranging

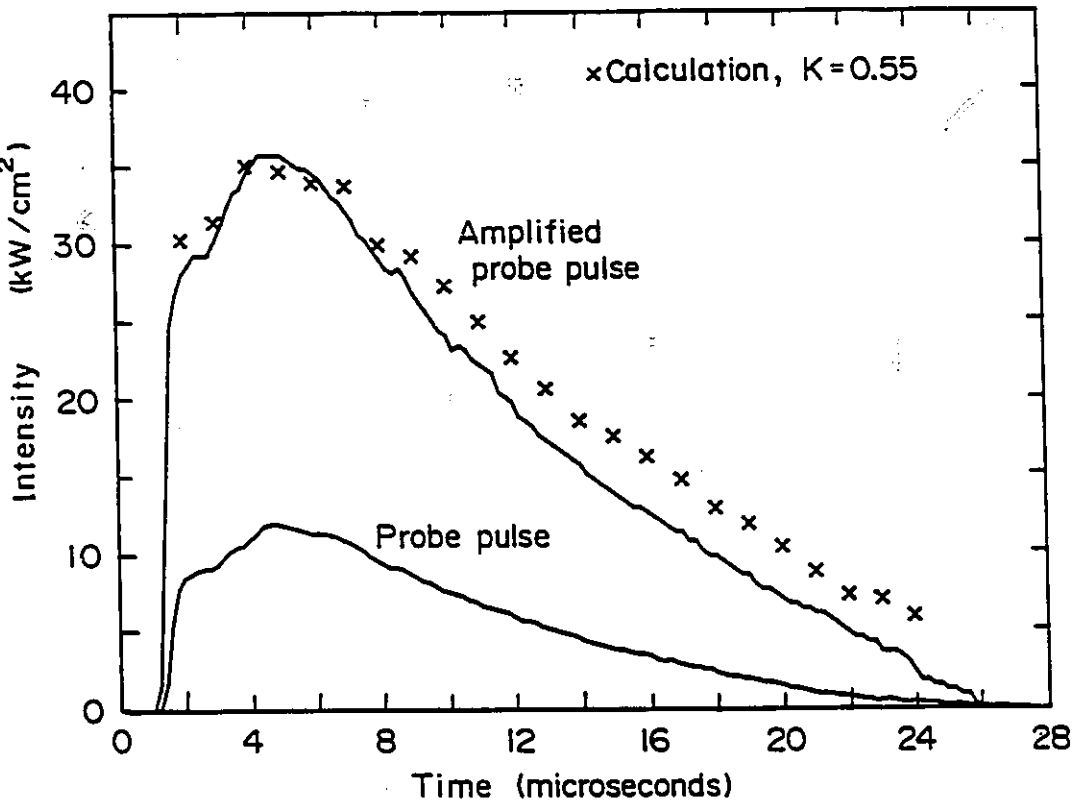


Figure 2.8: Repeat of Fig. 2.6 for a 120 cm amplifier cell operating at 200 K and 170 Torr. The gas mixture is 0.1% $NH_3$ in Ar. Theoretical points are calculated with K = 0.55

from 0.05% to 0.2% $NH_3$, gas temperatures ranging from 200 to 300 K, and for amplifier lengths of 60 and 120 cm. The measurements described in this section and the previous section provide confidence that the rate equation model can accurately predict amplifier performance throughout the parameter range of interest in the present study. Model predictions are discussed in the next section.

### 2.5 Discussion and Conclusions

The phenomenological constant, K, was introduced into the model to account for the experimental gain saturation results. The optimum value of K = 0.55 indicates

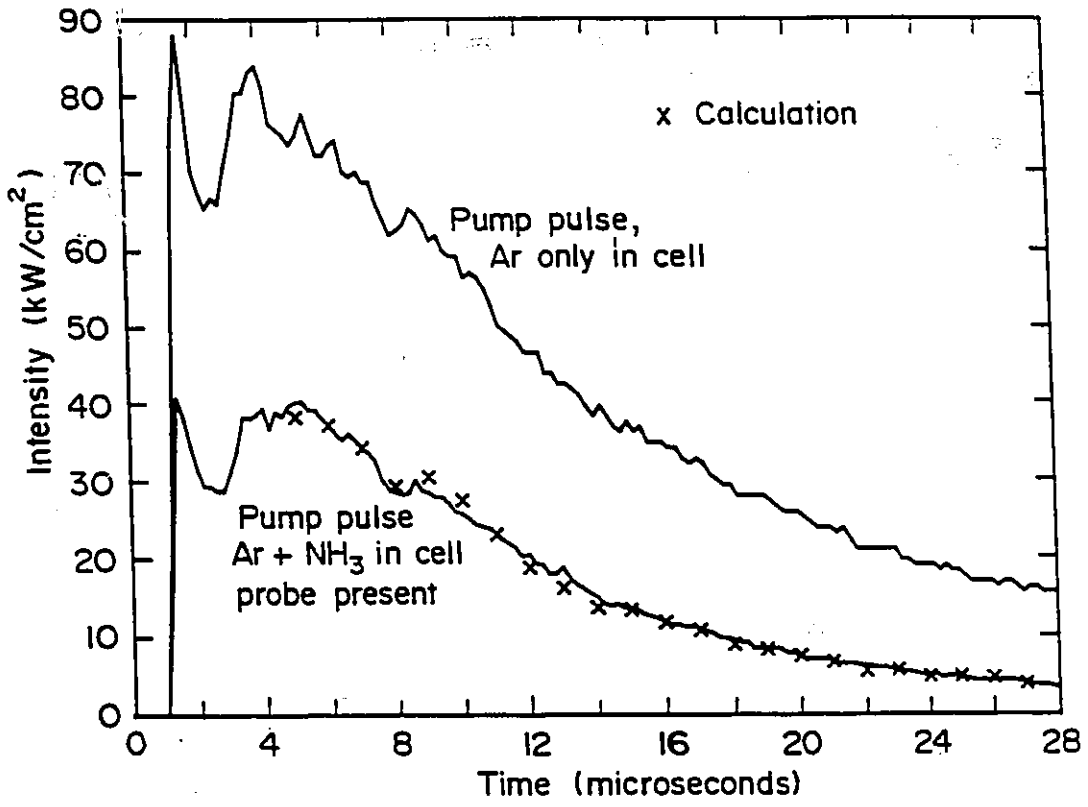


Figure 2.9: Attenuation of the 9R(30) pump pulse under conditions given in Fig. 2.8. Theoretical points are calculated with K = 0.55

that the transfer of energy between specific rotational energy levels may not proceed as fast as the collisional broadening rate. K may also account for the radial variation of the pump and probe intensities. All calculations are simply carried out using *average* intensities. In any event, the model with K = 0.55 gives good agreement with experiment.

### *A. Efficiencies*

Section 2.3 illustrates that large values of small-signal gain can easily be obtained in optically pumped $NH_3$, while Sect. 2.4 shows that efficient energy

extraction can also be achieved. Note that in Fig. 2.6 the peak probe intensity is amplified from 10 kW/cm$^2$ to 47 kW/cm$^2$, an increase of 37 kW/cm$^2$. Simultaneously, the pump intensity is reduced from 100 kW/cm$^2$ to 20 kW/cm$^2$, a reduction of 80 kW/cm$^2$. Thus the measured conversion efficiency is 46%. A probe intensity increase of 37 kW/cm$^2$ is equivalent to a power extraction of approximately 300 kW/l from the amplifier volume. For pulse lengths ≥30 $\mu$sec, energy extractions approaching 10 J/l can be attained, a significant increase over the 0.5 J/l reported by Deka *et al.* [30]. An alternative way of viewing the results shown in Figs. 2.6 and 2.7 is to calculate the number of $NH_3$ molecules which take part in the conversion of pump to probe radiation, if one assumes a single $NH_3$ molecule is required to produce one additional probe photon. At a 300 kW/l conversion rate, every $NH_3$ molecule in the gas (both ortho and para species) contributes once per microsecond, i.e., during the pulses shown in Figs. 2.6 and 2.7 approximately 10 probe photons are generated for every $NH_3$ molecule in the gas.

For optimum amplifier conditions, the model predicts overall power conversion efficiencies of 50% for operation at 200 K, and as high as 55% if the amplifier is cooled to 150 K (at room temperature, efficiency is reduced to 35%). Most of the pump radiation which is not converted into aQ(3,3) photons is used to maintain the population inversion against V-T collisions*, while a small percent of the pump photons exit the amplifier, even under optimum conditions. As window and waveguide losses are negligible in a well designed amplifier, experimental power efficiencies of 50% (equivalent to photon conversion efficiencies of ~60%) should be achievable.

---

*In dilute mixtures of Ar, the $NH_3$ V-T rate varies from 6090 Torr$^{-1}$ s$^{-1}$ at 300 K to 2393 Torr$^{-1}$ sec$^{-1}$ at 155 K [27,28]. This variation accounts for much of the reduction in efficiency as the amplifier is heated.

The optical pump for the $NH_3$ amplifier can be a multimode $CO_2$ pulse produced by a low or high pressure discharge, while the amplified aQ(3,3) signal can be a single mode Gaussian beam with a frequency bandwidth limited only by the pressure in the $NH_3$ amplifier. Thus, the pump laser can operate with poor mode quality, while the waveguide $NH_3$ amplifier will provide good mode quality and the desired bandwidth by conversion to aQ(3,3) radiation.

*B. Heating Effects*

The pump photons which are absorbed in the $NH_3$ gas eventually lead to gas heating. As the model gives an accurate representation of pump absorption (Fig. 2.7), it can be used to calculate gas heating. For dilute mixtures of $NH_3$, gas heating is proportional to the $NH_3$ concentration, and to the square of the total gas pressure. For a typical gas mixture of 0.1% $NH_3$ in 360 Torr Ar at 200 K, the rate of gas heating is ~1.5 K/$\mu$sec. Thus pulses of 20 to 30 $\mu$sec in length can be amplified before thermal effects become significant. If longer pulses are employed and gas heating is a concern, then larger amplifier cells (several metres) containing very dilute $NH_3$ (~0.01%) can be utilized. The optical pumping technique also allows a single pump laser to be split into several beams to pump a series of different waveguide amplifiers. These amplifiers can be separately optimised for amplification of weak pulses (pre-amp), as power amplifiers, or as wide bandwidth amplifiers (high pressure).

*C. Line-tunability*

Most of the experimental work in this chapter was carried out on the aQ(3,3) transition at 10.8 $\mu$m. A few measurements were made with the sP(3,0) transition at 11 $\mu$m. However, gain exists on many other ortho and para transitions in the $\nu_2$ band of $NH_3$. Reference [2] lists 65 transitions in $NH_3$ covering the wavelength region from

TABLE 2.3: Predicted performance of an $NH_3$ amplifier as a function of transition. Calculations are carried out for a 2-m amplifier containing 0.1% $NH_3$ in 170 Torr Ar at 200 K. It is assumed that the amplifier cell has negligible window and waveguide losses, and that the input intensities of the pump and probe are 100 kW/cm$^2$, and 10 kW/cm$^2$ respectively. (Figs. 2.6 and 2.7)

| Transition | Wavenumber [cm$^{-1}$] | Small-signal gain Coefficient [%/cm] | Power conversion efficiency [%] | |
|---|---|---|---|---|
| | | | Total [a] | Effective [b] |
| aQ(3,3) | 930.75697 | 8.4 | 46.4 | 64.6 |
| aQ(6,6) | 927.32300 | 4.5 | 38.7 | 60.7 |
| sQ(3,3) | 967.34631 | 5.3 | 33.4 | 59.2 |
| aP(4,0) | 853.81790 | 5.8 | 54.9 | 63.9 |
| aP(4,3) | 851.32685 | 3.3 | 51.2 | 62.5 |
| aP(7,3) | 796.13417 | 1.3 | 26.4 | 47.9 |
| aP(8,3) | 778.29002 | 0.55 | 10.9 | 30.6 |
| aP(9,3) | 760.69388 | 0.20 | 3.6 | 13.7 |
| sP(3,0) | 908.19912 | 4.7 | 45.7 | 63.2 |
| sP(5,3) | 867.71961 | 2.5 | 42.8 | 60.0 |
| sP(6,3) | 847.57811 | 1.8 | 34.7 | 55.1 |
| sP(7,3) | 827.48779 | 1.0 | 20.4 | 43.9 |
| sP(8,3) | 807.47174 | 0.44 | 8.4 | 26.4 |

[a] Defined as (Probe out - Probe in)/(Pump in)
[b] Defined as (Probe out - Probe in)/(Pump in - Pump out)

10.3 to 13.8 $\mu$m. Table 2.3 lists a few of the stronger transitions, and indicates typical amplifier performance for each transition. Clearly, the aQ(3,3) transition is one of the better transitions, but a similar performance can be obtained at several other wavelengths in the 11 - 12 $\mu$m region.

*D. Oscillator Performance*

This chapter has only dealt with the performance of optically pumped $NH_3$ as an amplifier. The rate equation model can also be used to predict the performance of a line-tunable $NH_3$ laser, and this is the focus of the work described in the following chapter.

# Chapter 3

## The Fundamental-Band Oscillator

### 3.0 Introduction

$NH_3$ lasers have been studied experimentally by several groups [4,5,31], with pulsed laser operation being observed between rotational levels of the ground state and the first excited $\nu_2$ vibrational level. Output energies of 1.5 J/pulse [4] and energy conversion efficiencies of 28% [5] have been measured with line-tunable output from 10 to 13 $\mu$m [32].

A simple laser configuration offering improved performance is reported in this chapter. This experimental configuration overcomes some of the limitations of previous work which required complicated configurations such as gratings at each end of the oscillator [4], a common output coupler for both the $CO_2$ and $NH_3$ lasers [5] or pumping into the cell off a grating [33]. In such configurations it is often difficult to change pump or emission wavelengths; a limitation not present in the current configuration. The line-tunable range of the regular $NH_3$ laser is extended to wavelengths longer than 14 $\mu$m by using a dilute mixture of $NH_3$ in a few hundred Torr of argon as the active medium.

### 3.1 Experimental Apparatus

Figure 3.1 is a schematic diagram of the experimental apparatus. The output of a TEA-$CO_2$ laser operating on the 9R(30) transition at 1084.635 $cm^{-1}$ is passed through a ZnSe dichroic mirror* and used to pump the oscillator. The typical pump

* The ZnSe dichroic mirrors were specially made to be > 90% transmitting in the 9 $\mu$m region and 98% reflecting in the 12 $\mu$m region.

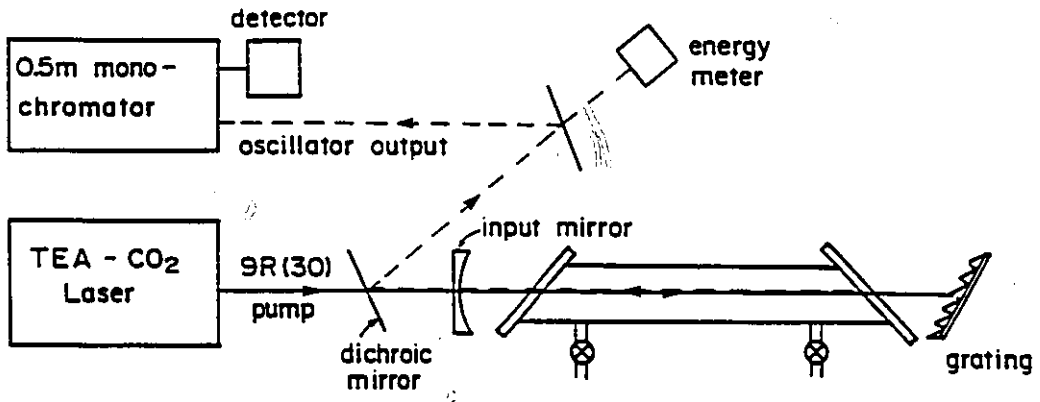


Figure 3.1: Schematic diagram of the $NH_3$ laser. A detailed description of the optics can be found in the text

pulse is ~3 $\mu$s long with a total energy of ~5 J and a peak intensity of 5 MW. The $NH_3$ oscillator contains a 1.5 m long quartz gas cell sealed with KCl Brewster windows. Inlet and outlet valves allow the gas mixture to be flowed continuously and hence the $NH_3$ concentration to be varied. The $NH_3$ laser cavity is formed by a concave ZnSe 30% reflecting mirror and a 79.35 lines/mm grating blazed at 35 degrees. The grating allows tuning to individual transitions. The output of the oscillator is taken through the ZnSe mirror and separated from the pump by the dichroic mirror. A Gen-Tec ED-500 Joulemeter is used to measure the pulse energy. A ¼ m monochromator and a AuGe or HgCdTe detector were used to verify single line oscillation and to determine the relative energies of competing lines.

### 3.2 Results

The model developed by Morrison *et al.* [17], as extended in Chapter 2, was used to predict the optimum values of input coupler, NH3 concentration, pressure and temperature for the maximum conversion efficiency on the strongest transitions [34].

These predictions were then checked experimentally using a range of input couplers, $NH_3$ concentrations, pressures and temperatures. As predicted by theory, an input coupler with reflectivity of ~30% was found to be optimum. The optimum $NH_3$ concentration, pressure and operating temperature were found to be transition dependent. For transitions characterized by $J < 7$ in the ground state, 0.2% $NH_3$ in Ar at a pressure of 170 Torr and temperature of 200 K was found to be optimum, while for higher J a temperature of 300 K and an increased pressure of 270 Torr optimised the energy conversion. The higher temperature increases the population in the higher J levels and results in increased gain. The higher pressure is also required to maintain the single pass pump absorption close to the optimum value of 60% [32]. For the highest J P-branch transitions observed, the concentration of $NH_3$ was increased to 0.5% in order to increase the single pass gain on these low gain transitions. The reflectivity of the input mirror was also increased to reduce the lasing threshold, and care was taken to select a grating with good efficiency in the 14 $\mu$m region.

The complete line-tunable results are summarized in Tables 3.1, 3.2 and 3.3. Table 3.1 groups the observed $NH_3$ transitions according to their energy conversion efficiency. The oscillator was pumped with a 5.2 J pump pulse at both 200 K and 300 K. For a number of the lower sP transitions, the monochromator had insufficient power to separate the individual transitions. Thus, these transitions are denoted with an unspecified value of K. Table 3.2 lists the transitions in order of decreasing wavenumber and gives the measured conversion efficiencies. Transitions for which the oscillator grating resolution was not sufficient to ensure single line operation are grouped together with unspecified K. The aP lines could be resolved by the monochromator and thus it was often possible by tuning of the oscillator grating to obtain 95% of the output on individual transitions. In both Tables 3.1 and 3.2, the

Table 3.1: Summary of the observed $NH_3$ transitions arranged according to the energy conversion efficiencies (See text for experimental conditions)

| Energy conversion efficiency | | | |
|---|---|---|---|
| **low 1-5%** | **medium 5-10%** | **high 10-20%** | **very high > 20%** |
| aR(2,2) | aQ(2,2) | aP(2,0) | sP(3,K) |
| aR(1,1) | aQ(3,3) | sP(4,K) | sP(5,K) |
| sQ(2,2) | aQ(5,5) | aP(3,1) | aP(4,0) |
| sQ(4,3) | aQ(6,6) | aP(3,2) | aP(5,3) |
| sQ(4,4) | aP(2,1) | aP(4,3) | |
| sQ(5,5) | aP(4,1) | sP(6,K) | |
| aQ(4,3) | aP(4,2) | aP(5,1) | |
| aQ(4,4) | aP(6,1) | aP(5,2) | |
| sP(2,1) | aP(6,2) | aP(5,4) | |
| aR(0,0) | aP(6,5) | sP(7,K) | |
| sP(1,0) | aP(7,2) | aP(6,0) | |
| sP(8,K) | aP(7,5) | aP(6,3) | |
| sP(8,6) | aP(8,3) | aP(6,4) | |
| aP(7,1) | aP(8,6) | aP(7,3) | |
| aP(7,4) | | aP(7,6) | |
| sP(9,3) | | | |
| sP(9,6) | | | |
| aP(8,0) | | | |
| aP(8,1) | | | |
| aP(8,4) | | | |
| aP(8,5) | | | |
| aP(8,7) | | | |
| aP(9,3) | | | |
| aP(9,6) | | | |

energy conversion efficiency is calculated as the $NH_3$ pulse energy divided by the 9R(30) $CO_2$ pulse energy measured *before* the oscillator. From this efficiency, the internal conversion efficiency and the photon conversion efficiency can also be calculated. For example, on the aP(4,0) transition, pulses of 1.5 J were recorded from a 5.2 J pump pulse, giving an energy conversion efficiency of 29% (see Table 3.2). To calculate the internal energy conversion efficiency, one must recognize that only

Table 3.2: Efficiency of $NH_3$ laser operation arranged according to descending wavenumber. Experimental conditions are summarized in the text. The energy conversion efficiency is defined as the measured $NH_3$ pulse energy divided by the 9R(30) $CO_2$ energy incident on the input mirror

| $NH_3$ Transition | Wavenumber [$cm^{-1}$] | Efficiency [%] | |
|---|---|---|---|
| | | 200 K | 300 K |
| aR(2,2) | 992 | 2.1 | 1.4 |
| aR(1,1) | 972 | 2.3 | 3.6 |
| sQ(2,2) | | | |
| sQ(4,3-4) | 967 | 7.0 | -- |
| sQ(5,5) | | | |
| aQ(4,3-4) | | | |
| aQ(2,2) | 931 | 19 | 16 |
| aQ(3,3) | | | |
| aQ(5,5) | 929 | | |
| sP(2,1) | 928 | 13 | 15 |
| aQ(6,6) | 927 | | |
| aQ(6,6) | 927 | 8.0 | -- |
| aR(0,0) | 952 | -- | 1.1 |
| sP(1,0) | 948 | -- | 0.8 |
| sP(3,K) | 908 | 25 | 18 |
| aP(2,K) | 892 | 21 | 15 |
| sP(4,K) | 888 | 19 | 16 |
| aP(3,1) | 873 | 13 | 7.7 |
| aP(3,2) | 872 | 10 | -- |
| sP(5,K) | 868 | 28 | 22 |
| aP(4,K) | 851-854 | 29 | 21 |
| sP(6,K) | 847-848 | 19 | 17 |
| aP(5,K) | 833-835 | 19 | 16 |
| aP(5,3) | 833 | 23 | 18 |
| aP(5,4) | 831 | 11 | 7.5 |
| sP(7,K) | 826-828 | 18 | 18 |
| aP(6,0-1) | 816 | 24 | 18 |
| aP(6,2-3) | 815 | 18 | -- |
| aP(6,3) | 814 | 20 | 14 |
| aP(6,4) | 812 | 13 | 8.6 |
| aP(6,5) | 810 | 8.2 | 4.4 |
| sP(8,K) | 806-808 | 3.3 | 6.7 |
| sP(8,6) | 806 | 2.4 | 4.2 |

Table 3.2: Efficiency of $NH_3$ laser operation arranged according to descending wavenumber (continued)

| $NH_3$ Transition | Wavenumber [$cm^{-1}$] | Efficiency [%] | |
|---|---|---|---|
| | | 200 K | 300 K |
| aP(7,1-2) | 798 | 6.1 | 6.4 |
| aP(7,3) | 796 | 11 | 8.5 |
| aP(7,4) | 794 | 3.5 | 4.1 |
| aP(7,5) | 792 | 5.7 | 4.6 |
| aP(7,6) | 789 | 12 | 11 |
| sP(9,K) | 786-788 | -- | 2.9 |
| sP(9,6) | 786 | -- | 1.5 |
| aP(8,0-1) | 780-781 | 2.8 | 5.7 |
| aP(8,3) | 778 | 4.6 | 7.2 |
| aP(8,4) | 776 | 0.9 | 2.1 |
| aP(8,5) | 774 | 1.5 | 2.7 |
| aP(8,6) | 771 | 8.0 | 8.6 |
| aP(8,7) | 767 | -- | 1.8 |
| aP(9,3) | 761 | 0.3 | 1.8 |
| aP(9,5) | 757 | -- | 0.7 |
| aP(9,6) | 754 | 0.5 | 2.7 |
| aP(9,7) | 750 | -- | 0.5 |

70% of the pump energy enters the oscillator, and 15% of this energy passes through the gas unabsorbed and is diffracted off the grating at the other end. Thus only 3.1 J of the 5.2 J incident on the oscillator is actually absorbed in the gas. Of this absorbed energy, ~50% is converted to 12 $\mu$m photons. As the quantum efficiency for the aP(4,0) transition is 0.79, this energy conversion corresponds to a photon conversion efficiency of greater than 60%. The remainder of the energy goes into gas heating. Similar high photon conversion efficiencies are also observed on other lines. (A similar calculation for the aP(5,3) transition yields a photon conversion efficiency of 52%.)

In Table 3.3, the newly observed high-J transitions are listed, along with their respective wavenumbers. Although these transitions are weak, they are important in

Table 3.3: Summary of observed long wavelength transitions. The efficiency of these weak transitions was < 1% (See text for experimental conditions)

| $NH_3$ Transition | Wavenumber [$cm^{-1}$] |
|---|---|
| sP(9,3) | 787.58 |
| sP(9,6) | 786.19 |
| sP(10,6-9) | 764-766 |
| aP(9,5) | 756.58 |
| aP(9,7) | 749.86 |
| sP(11,K) | 744-749 |
| aP(10,0) | 745.42 |
| aP(9,8) | 745.29 |
| aP(10,3) | 743.31 |
| aP(10,4) | 741.62 |
| aP(10,5) | 739.37 |
| aP(10,6) | 736.51 |
| aP(10,7) | 732.94 |
| aP(11,3) | 726.13 |
| aP(10,9) | 723.27 |
| aP(11,6) | 719.64 |
| aP(11,9) | 707.05 |

that they extend the tunability range of the $NH_3$ laser to wavelengths longer than 14 $\mu$m.

To determine the maximum efficiency of the $NH_3$ oscillator, the configuration was changed slightly. The ZnSe input mirror was removed and replaced by a dichroic mirror to ensure high transmittance of the pump radiation and a high reflectance at the input end of the oscillator. The grating also was removed and replaced with a concave 30% reflecting output mirror. Behind the output mirror a second dichroic mirror was used to separate the $CO_2$ pump radiation from the $NH_3$ radiation. In order to maximize the energy output and to test the scalability of the system, the pump energy was increased to 13 J.

Using this non-wavelength selective cavity, an energy output of 4.6 J/pulse at 12 $\mu$m was observed, corresponding to a total energy conversion efficiency of 35%

($NH_3$ laser output/$CO_2$ laser output). These results demonstrate the scalability of the system to higher input energies.

### 3.3 Conclusions

The previous 2 chapters have studied "conventional" $NH_3$ amplifiers and oscillators. While chapter 2 explored the amplification characteristics of the ammonia medium in both the small signal and staturated gain modes, this chapter shows that a very simple laser configuration containing a dilute mixture of $NH_3$ in Ar provides high energy line-tunable output in the 10 to 14 $\mu$m region. The next 2 chapters complete the present study by looking at amplification at high pressures and the operation of the hot-band ammonia laser.

# CHAPTER 4

## High Pressure Amplifier Operation

### 4.0 Introduction

Chapters 2 and 3 have shown $NH_3$ oscillators and amplifiers operating at pressures well below one atmosphere to be efficient converters of 9 $\mu$m $CO_2$ radiation to radiation in the 10 to 14 $\mu$m region [4,5,34,35]. Previously only preliminary work has been carried out to characterize the behaviour of $NH_3$ amplifiers and oscillators at pressures exceeding 1 atmosphere [19,36,37], and the performance of such systems has been far from optimum.

The chief advantage of operating optically pumped mixtures above one atmosphere is the increased bandwidth available at higher pressures. At pressures of several atmospheres, the pressure broadened bandwidth allows for continuous tunability over large segments of the 800 - 1000 $cm^{-1}$ region, and enables amplification or generation of short laser pulses. Currently, much of the work on generating picosecond pulses in the mid-infrared has centred on the development of multi-atmosphere-discharge-excited $CO_2$ lasers [38]. However, there are several problems associated with high pressure discharge systems. These problems include discharge instabilities (arcs), damage to incavity optics, and the requirement for very high voltages. In light of these concerns, optical pumping of high pressure $CO_2$ has recently been suggested as an alternative approach [39].

In this chapter, optical pumping as a technique for generating large gain-bandwidth in the 10 $\mu$m region is examined with $NH_3$ as the infrared active gas, rather than $CO_2$. The $NH_3$ system has gain in regions overlapping the 10.6 $\mu$m $CO_2$ band and for optical pumping, the polar $NH_3$ molecule possesses several advantages

relative to $CO_2$. A set of rate equations was developed to model the $NH_3$ system, and the model verified by experimental measurements at a number of frequencies, pressures, concentrations and temperatures. Experimentally, single pass gains of 150 (21.8 dB) are observed in dilute $NH_3$ mixtures at 6 atmospheres for the 10P(34) $CO_2$ transition. At this pressure the gain bandwidth in $NH_3$ is ~4 $cm^{-1}$, suitable for amplifying pulses as short as a few picoseconds. Measurements indicate that optically pumped $NH_3$ is a viable alternative to multi-atmosphere $CO_2$ discharge amplifiers for many applications.

### 4.1 Model

A rate equation approach has been used successfully to model the behaviour of $NH_3$ systems operating at pressures below one atmosphere [17,34, see chapter 2]. The rate equation approach involves balancing the rate of molecules pumped up from the ground state to the $\nu_2 = 1$ level of $NH_3$ with the rate of molecules decaying via collisional relaxation and stimulated emission. The rate equation approach is illustrated in Fig. 4.1. The $NH_3$ energy levels can be represented by a series of anharmonic vibrational levels, upon which rotational levels are superimposed. In an exact treatment, each of these vibrational-rotational levels must be handled individually. However, for dilute mixtures (low concentrations) of $NH_3$, fast rotational relaxation rates ensure that only small perturbations from the thermal rotational distribution can occur within a given vibrational level. Thus, a simple model which assumes that the rotational populations within a vibrational level are always in thermal equilibrium was developed*. Optical pumping by the 9R(30) $CO_2$ transition transfers population to the $\nu_2 = 1$ vibrational level. The relaxation of this

* Detailed calculations which separate out the directly pumped levels from the rotational "bath" [34] indicate that, under the experimental conditions used in this paper, any population deviations are < 10% of the thermal equilibrium value.

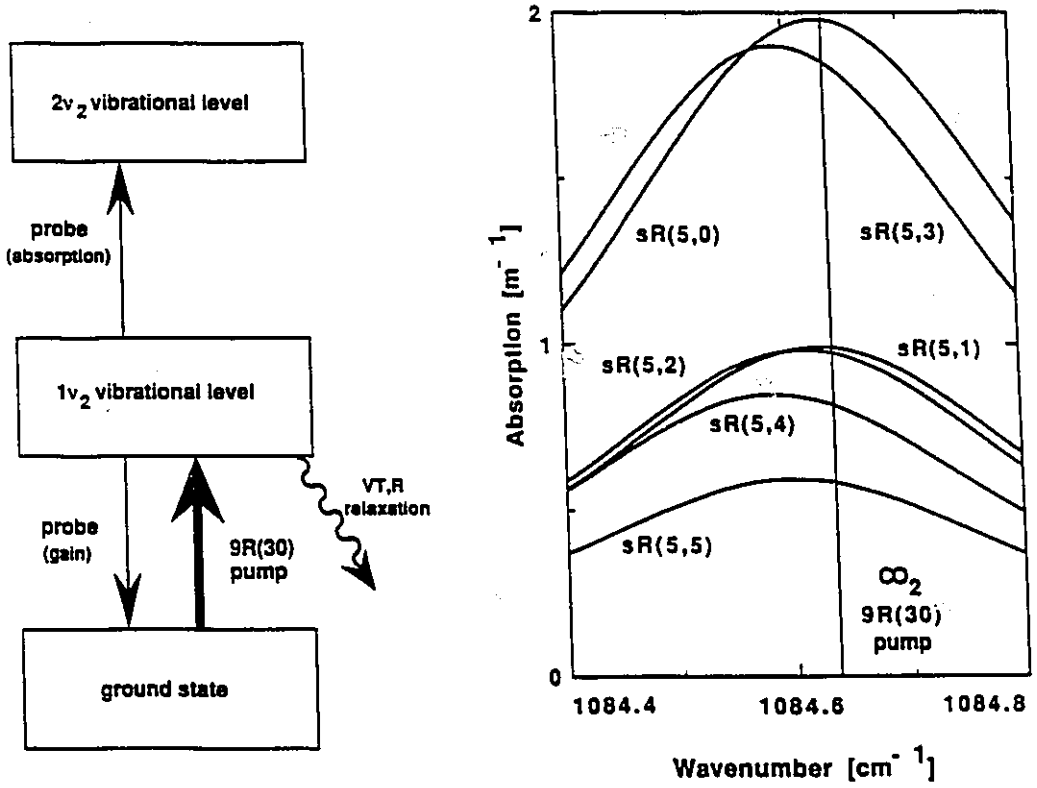


Figure 4.1: Illustration of the relevant vibrational energy levels and spectroscopy of the $NH_3$ laser. The $CO_2$ 9R(30) pump transfers population from the ground state to the $1\nu_2$ vibrational level. Relaxation back to the ground state is dominated by VT,R collisions. The probe radiation interacts with transitions in both the ($1\nu_2 \leftarrow$ gs) and ($2\nu_2 \leftarrow 1\nu_2$) bands. Also shown are calculated spectra for the individual pressure broadened transitions in the sR(5,K) multiplet. The spectra are calculated for a concentration of 0.1% $NH_3$ in 2 atm of $N_2$ at 200 K. The line at 1084.635 $cm^{-1}$ indicates the position of the 9R(30) $CO_2$ pump transition

population back to the ground state is dominated by vibrational-translational (VT,R) relaxation processes. The model calculates the instantaneous population in the $\nu_2$ = 1 vibrational level, and uses this population to calculate the gain on individual rotational-vibrational transitions between the ground state and the $\nu_2$ =1 vibrational

level. To account for high pressure operation, the model considers each transition to have the appropriate pressure broadened Lorentz lineshape, and sums the contributions from overlapping lines. The possibility of absorption due to transitions from the $\nu_2 = 1$ to $\nu_2 = 2$ vibrational levels must also be considered [37]. These hot-band transitions overlap the region of gain for the $\nu_2 = 1$ band, and hot-band absorption reduces or eliminates gain at many wavelengths. The model calculates this absorption and subtracts it from the gain calculated for the ground state to $\nu_2 = 1$ transitions.

For each of the two vibrational bands included in the model, the ortho and para species of $NH_3$* are treated separately. The collisional transfer of energy between the two species is slow [26], and is ignored in the present model. However, at high pressure the 9R(30) $CO_2$ radiation pumps transitions in both ortho and para $NH_3$. As can be seen in Fig. 4.1, the *total* absorption of the pump radiation by ortho and para transitions are approximately equal, and, as a consequence, each species produces a similar level of inversion**. The total pump absorption and probe amplification is calculated by summing the contributions from ortho and para species in the ($1\nu_2 \leftarrow$ gs) and ($2\nu_2 \leftarrow 1\nu_2$) bands.

The equations given below are the rate equations which are used to calculate the population in the three vibrational levels shown in Fig. 4.1. These equations are applied separately to ortho- and para-$NH_3$.

---

*In ortho-$NH_3$, the quantum number of the component of angular momentum along the molecular axis, K, is equal to 3n [where n is zero or a positive integer], while for para-$NH_3$ $K = 3n \pm 1$. Thus sR(5,0) and sR(5,3) are ortho-transitions, while sR(5,1), sR(5,2), sR(5,4) and sR(5,5) are para-transitions.

**A very different behaviour is observed when pumping low pressure $NH_3$ mixtures [cf chapter 2]. With the 9R(30) $CO_2$ pump, only ortho $NH_3$ is inverted. An alternative pump wavelength must be used to invert the para species [2]

$$\frac{dN_0}{dt} = -\frac{dN_1}{dt} = \frac{N_1 - A \times N_0}{\tau_{VT}} - P \qquad (4.1)$$

$N_0$ and $N_1$ represent the populations in the ground state and $\nu_2 = 1$ level. The population of the $\nu_2 = 2$ level, $N_2$, is considered to remain in thermal equilibrium with the $\nu_2 = 1$ level [24], and it is assumed that $N_0+N_1+N_2 = N$, the total population (i.e., only the three levels shown in Fig. 4.1 contain significant population). In equation (1), A is the thermal equilibrium ratio of $N_1/N_0$ and $\tau_{VT}$ is the VT,R relaxation rate from the $\nu_2 = 1$ vibrational level to the ground state. The pumping term, P, is the rate of optical pumping of molecules into the first vibrational level from the ground state. This rate is the sum of the pumping on the individual transitions. In the case of ortho-$NH_3$, the overall rate involves summing the overlapping absorptions from the sR(5,0) and sR(5,3) transitions. The individual pumping rates are given by:

$$P_i = \frac{I_p(t)}{h\nu_p} \times \alpha_i(\nu_p) \qquad (4.2)$$

$I_p(t)$ is the intensity of the pump pulse, $h\nu_p$ is the energy per photon at the pump frequency ($\nu_p$), and $\alpha$ is the absorption at the pump frequency for a given transition. The absorption is given by:

$$\alpha(\nu) = \sigma(\nu) \times \left( f_l \times N_0 - f_u \times N_1 \times \frac{g_l}{g_u} \right) \qquad (4.3)$$

where $\sigma(\nu)$ is the absorption cross-section for the transition at frequency $\nu$; $f_l$ and $f_u$ are the fraction of molecules in the lower and upper rotational levels of the pumped transition, while $g_l$ and $g_u$ are their respective degeneracies.

Equations (4.1 - 4.3) are solved numerically for $N_1/N_0$ as a function of time. The calculated values of $N_1/N_0$ are then used to determine the gain on the individual transitions. In addition, a knowledge of the ratio $N_1/N_0$ allows one to calculate the hot-band absorptions since the $2\nu_2$ vibrational level can be assumed to be in thermal equilibrium with the $1\nu_2$ vibrational level (i.e., at 200 K, $N_2 = 0.0062\ N_1$ [44]). The contributions from all transitions are then summed to give the total overlapping gain or absorption at the pump and probe frequencies. This sum is carried out by assuming that all rotational-vibrational transitions have the same pressure broadening coefficient. This assumption is based on the work of Beckwith *et al.* [29], who measured the relevant pressure broadening coefficients on a number of $NH_3$ transitions and determined that the values agreed within ± 20 %. Table 4.1 lists the molecular constants used in the model.

As the pump beam propagates down the amplifier cell, its intensity decreases due to absorption. This depletion in pump intensity is given by:

$$\frac{dI_p(x,t)}{dx} = -\alpha(x,t,\nu_p) \times I_p(x,t) \qquad (4.4)$$

where $\alpha(x,t,\nu_p)$ is the absorption of the pump radiation due to all $NH_3$ transitions. To evaluate the total gain in the cell this attenuation of the pump is taken into account by splitting the gain cell into small sections and calculating the gain and pump absorption for each section.

Figure 4.2 shows the results obtained by calculating gain for a short $NH_3$ cell pumped at 25 MW/cm$^2$ - a typical experimental pump intensity. In the 800 to 1000

Table 4.1: Physical constants used in the modelling of high pressure $^{14}NH_3$ amplifiers.

VT,R Relaxation rates [$\mu s^{-1}$ $Torr^{-1}$]

| Collision Partner | Temperature | |
|---|---|---|
| | 200 K | 300 K |
| $NH_3$ | 1.14 [a] | 1.45 [a] |
| Ar | 0.0035 [b] | 0.0059 [c] |
| $N_2$ | 0.0075 [a] | 0.0102 [a] |

Dipole moments for $\nu_2$ band [D]

| Transition | Dipole |
|---|---|
| 1a ← 0s | 0.237 [d] |
| 1s ← 0a | 0.244 [d] |
| 2a ← 1s | 0.28 [e] |
| 2s ← 1a | 0.42 [e] |

Pressure broadening coefficients [MHz/Torr]

| Buffer gas | Temperature | |
|---|---|---|
| | 200 K | 300 K |
| $NH_3$ | [f] | [g] |
| Ar | 4.9 [f] | 3.5 [d] |
| $N_2$ | 2.0 [f] | 1.5 [d] |

[a] Danagher and Reid [ref. 26]
[b] Hovis and Moore [ref. 28]
[c] Hovis and Moore [ref. 27]
[d] Beckwith, Danagher and Reid [ref. 29]
[e] Dubé and Reid [ref. 24]
[f] pressure broadening at 200 K is estimated from the broadening coefficients at 300 K using the relationship given by Townes and Schawlow [ref. 20]: where T is the temperature and n = 1 for $NH_3$-$NH_3$ collisions, n = 7 for Ar-$NH_3$ collisions and n=4 for $N_2$-$NH_3$ collisions.
[g] calculated for each transition from equation developed by Morrison in Appendix C of his thesis [ref. 15] based on Table 2 of Taylor [ref. 40]

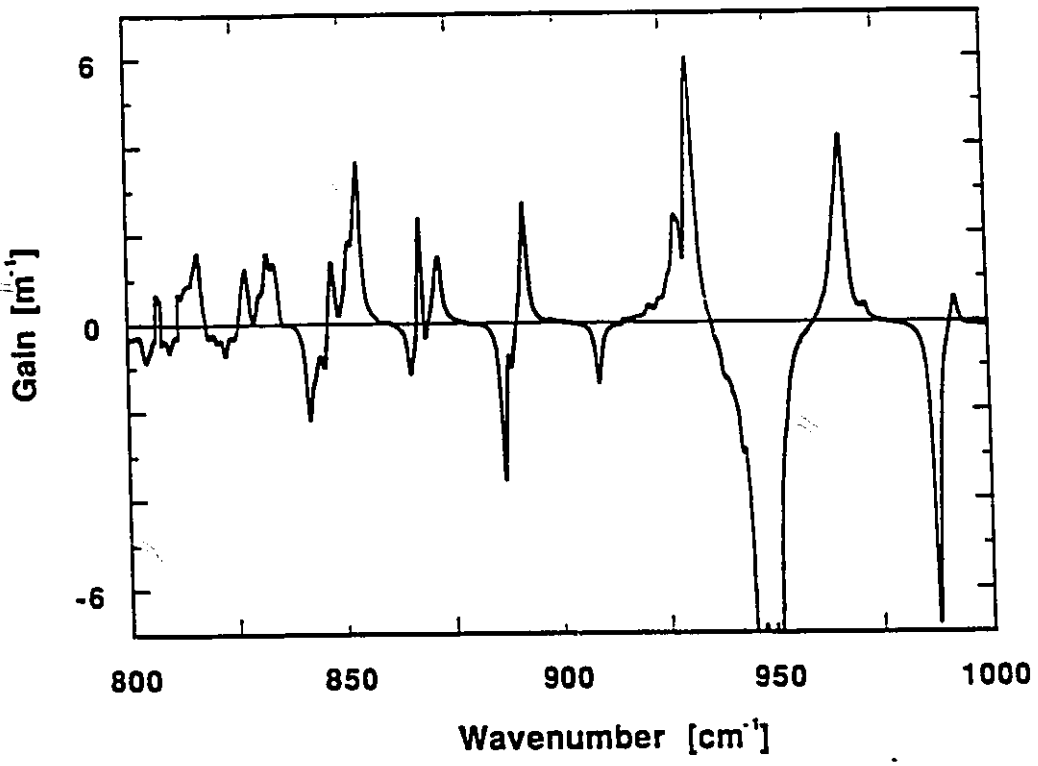


Figure 4.2: Calculated gain and absorption in $NH_3$ for a peak pump intensity of 25 MW/cm$^2$. The calculation is carried out for a 0.12 % $NH_3$ in $N_2$ mixture at 6.33 atm and 200 K

cm$^{-1}$ region there are significant areas of both gain and absorption. The absorbing regions are a result of the transitions from the $1\nu_2$ to $2\nu_2$ level. Figure 4.2 clearly demonstrates the importance of including hot band transitions in the model. Any model which calculates gain based solely on the regular band transitions will greatly overestimate the extent of gain in a high pressure system. (The importance of the overlying hot-band was first pointed out by Morrison *et al.* [37].) From Fig. 4.2, it is clear that the model calculations predict maximum gain in the region from 926 to 938 cm$^{-1}$ while the region of strongest absorption is from 938 to 955 cm$^{-1}$. This strong absorption is caused by the overlapping sQ-branch transitions of the hot-band,

while the gain at 932 $cm^{-1}$ is due to the overlapping aQ-branch transitions of the regular band. The fact that the regions of maximum gain and absorption are associated with Q-branch transitions is very significant from a modelling point of view, as Morrison *et al.* [17] have shown that the exact value of gain or absorption in the Q-branch is extremely sensitive to the value of $N_1/N_0$.

Thus, the wavelength region from 926 to 955 $cm^{-1}$ provides both the largest experimental signals, and the most sensitive test of the model predictions. Therefore, this wavelength region was selected for these experiments, and, in the next section, the experimental apparatus is described for making small-signal gain measurements in the 926 to 955 $cm^{-1}$ region.

### 4.2 Experimental Apparatus

Figure 4.3 is a schematic of this experimental apparatus. A TEA-$CO_2$ laser operating on the 9R(30) transition was used to pump a high pressure $NH_3$ cell. The gas mixture in the pump laser was adjusted to provide a 100 ns FWHM pulse with minimal tail. For the probe laser, a second TE-$CO_2$ laser operating at 400 Torr provided a relatively long pulse, as shown in Fig. 4.4. Thus, under the typical experimental conditions, the pump-induced gain or absorption can be measured from a single trace. By line-tuning the probe laser from 10P(8) to 10P(38), the wavelength region of interest can easily be covered. The $NH_3$ cell (Fig. 4.3) typically contained a mixture of $< 0.1\%$ $NH_3$ in a buffer gas. A dichroic mirror and grating were used to separate the probe and pump pulse. A gas cell filled with $CF_3I$ was placed before the probe detector to absorb residual 9 $\mu$m radiation. Both the pump and probe pulses were detected using Au:Ge detectors. The signals from the detectors were recorded by a fast digital oscilloscope (10 ns per point). 50 successive pulses were averaged, and the resultant trace transferred to a computer for analysis.

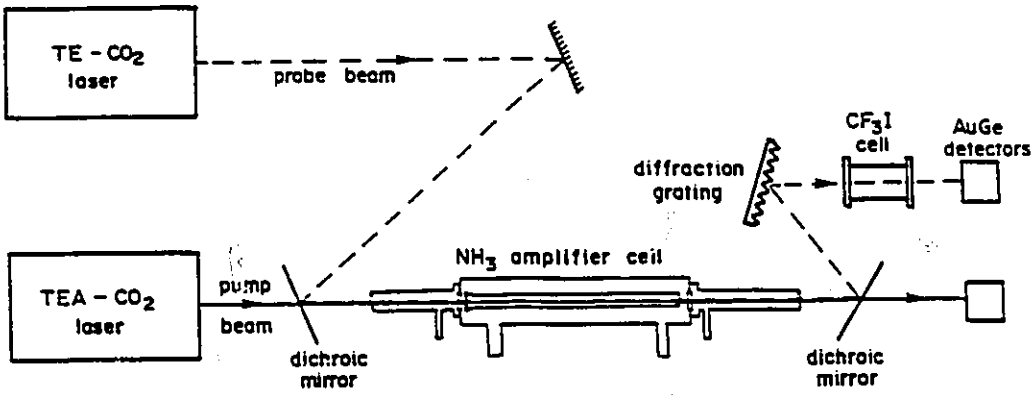


Figure 4.3: Schematic diagram of the apparatus for measuring gain in high pressure $NH_3$ mixtures. The high pressure $NH_3$ amplifier is comprised of a pyrex waveguide surrounded by an aluminum cylinder. It is designed with pyrex extension tubes to ensure that the cold salt windows do not come into contact with the moist room air. In addition the pyrex extension at the input acts as a spatial filter to eliminate hot spots in the pump beam

### 4.3 Results

Figure 4.5 is an example of the type of measurement taken in comparing calculations and experimental results. The 10P(36) $CO_2$ pulse probes an area of the spectrum dominated by $1\nu_2 \leftarrow$ gs transitions. Thus, in the absence of the 9R(30) pump the probe experiences absorption. However, with the 9R(30) pump travelling collinearly, the population is inverted and a gain spike appears on the 10P(36) $CO_2$ pulse. As the collisional relaxation time is 22 nanoseconds, the gain quickly decays after the pump pulse. Model calculations agree closely with experimental measurements at the peak and exhibit reasonable agreement in the tail of the pump pulse.

As it is relatively simple to grating-tune the $CO_2$ probe laser, measurements were also made on the $CO_2$ lines surrounding 10P(36). Figure 4.6 summarizes the results of these measurements and compares them with calculations. The lower trace

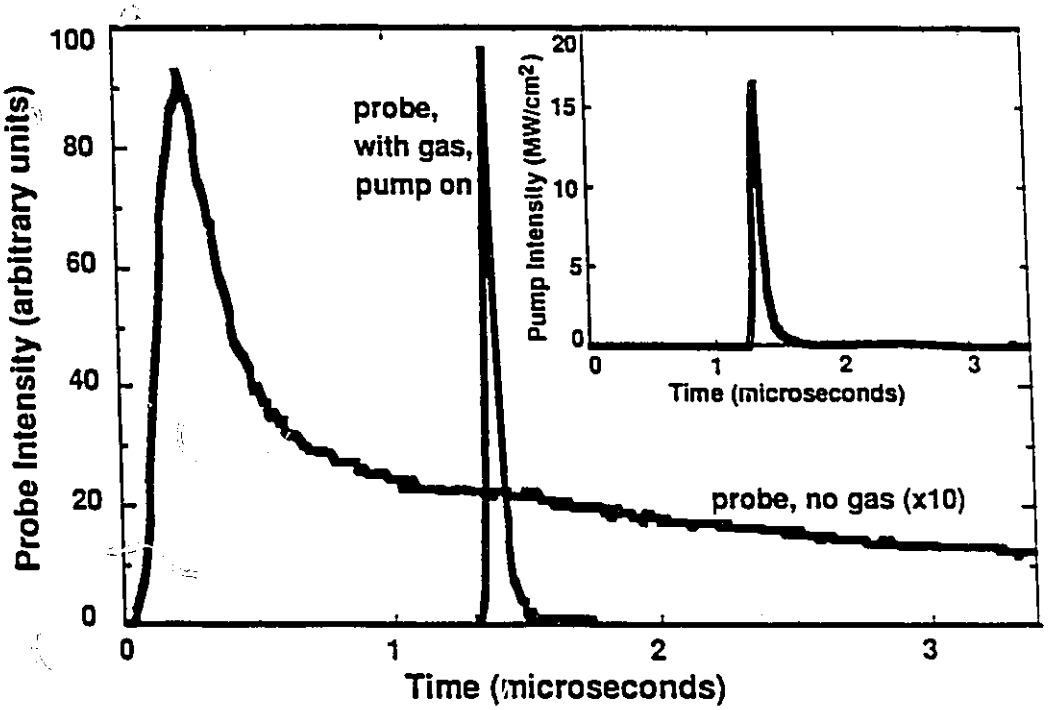


Figure 4.4: Typical probe and pump pulses used in the experiment. The inset shows the 9R(30) pump pulse, while the main traces show the 10P(34) probe pulse, both with and without amplification in a 0.1 % $NH_3$ in $N_2$ mixture at 5.3 atm and 200 K. At the peak of the pump pulse, the probe is amplified by a factor of 45. The cell length is 88 cm

compares the absorption measured by passing *only* the probe through the amplifier with that calculated from the model. The good agreement between calculations and experiment serves as a check on both the pressure broadening coefficients and the experimental $NH_3$ concentration. The concentration is determined using calibrated flowmeters. The upper trace in Fig. 4.6 demonstrates the excellent agreement between experiment and theory at the peak of the pump pulse. The experimental $NH_3$ concentration was chosen so that both gain and absorption could be measured at the same time. Thus on 10P(34), we were able to observe an absorption of 6%/cm change into a gain of 2%/cm when the 9R(30) pump pulse was present. Moving across the

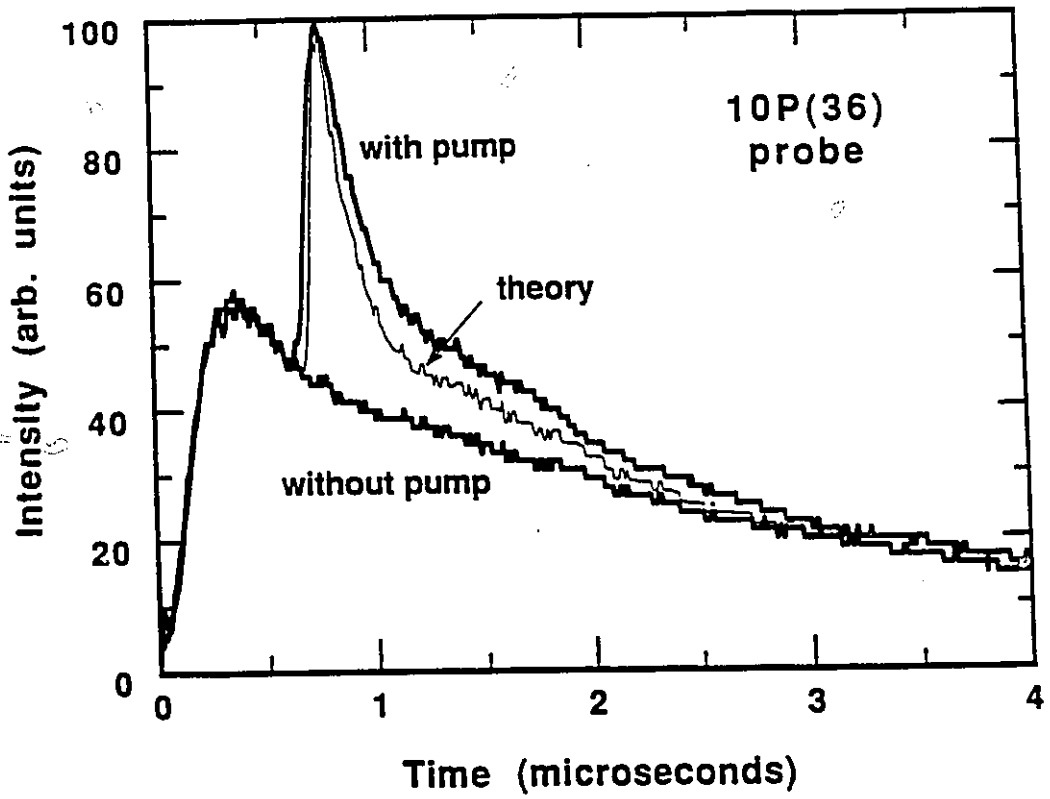


Figure 4.5: Comparison between theory and experiment for the amplification of a 10P(36) $CO_2$ probe pulse. The $NH_3$ concentration is 0.007% $NH_3$ in 8.33 atm of $N_2$ at 200 K. The peak pump intensity is 8.4 MW/cm$^2$ at the input to the 88 cm cell

profile, gain is seen to vary from 1%/cm on those transitions with the strongest absorptions to zero on those with weak absorptions in accord with calculations. The bandwidth of the gain is ~ 4 cm$^{-1}$. This bandwidth is sufficient to amplify a $CO_2$ laser pulse as short as a few picoseconds.

As seen in Fig. 4.2, in addition to predicting regions of strong gain, the model also predicts regions of strong absorption, particularly around 950 cm$^{-1}$. This region was probed using the 10P(14) $CO_2$ transition and the results are shown in Fig. 4.7. In contrast to the gain seen on 10P(36), 10P(14) experiences greatly increased absorption in the presence of the pump pulse. This increased absorption is evident well into the

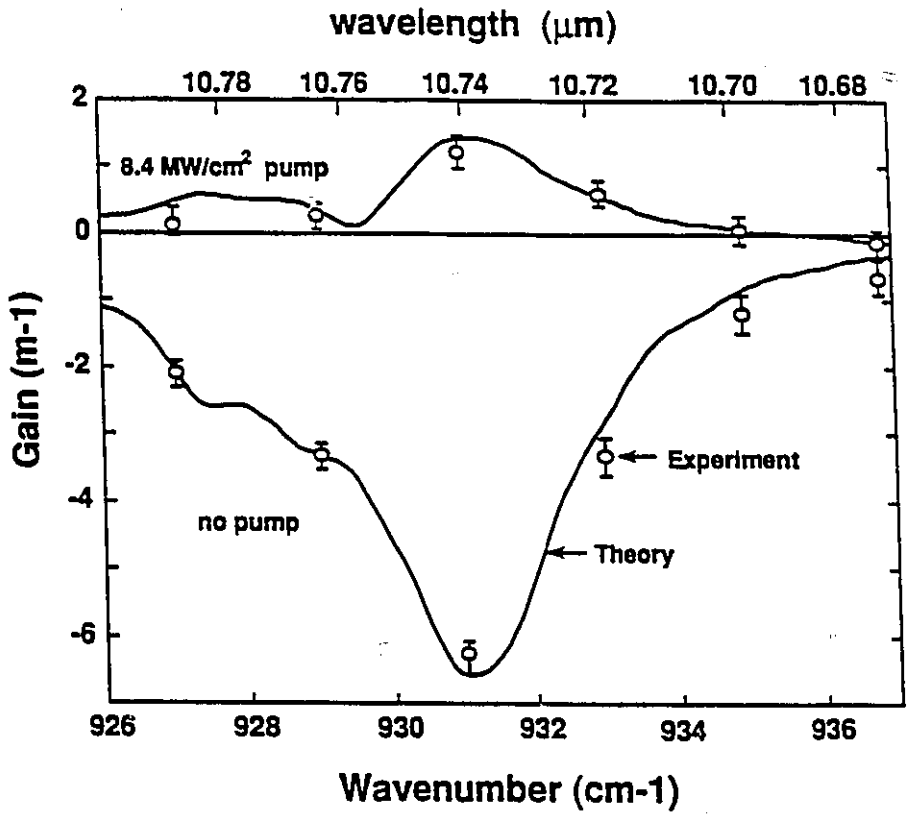


Figure 4.6: Comparison of theory and experiment for measurements made at six different $CO_2$ probe transitions. The theoretical lines are calculated for a mixture of 0.04 % $NH_3$ in 5.5 atm of $N_2$ at 200 K, pumped with a peak intensity of 8.4 MW/cm$^2$. The measured points are obtained with and without the pump beam in the cell

tail of the pump pulse and is quite sensitive to the actual value of the pump intensity (The second drop in transmission is due to an increase in intensity in the tail of the 9R(30) pump pulse).

Tuning the probe laser around the 10P(14) transitions enabled the tracing out of the pump-induced absorption profile in this region. The results of these measurements are compared with model calculations in Fig. 4.8. In contrast to Fig. 4.6, the upper trace represents the absorption with the pump absent. The lower trace indicates the absorption at the peak of the pump pulse. Here, as in Fig. 4.6, the main sources of experimental error are due to fluctuations in concentration, pulse-to-pulse variations in the pump pulse shape, and digitalization inaccuracies. In the case of

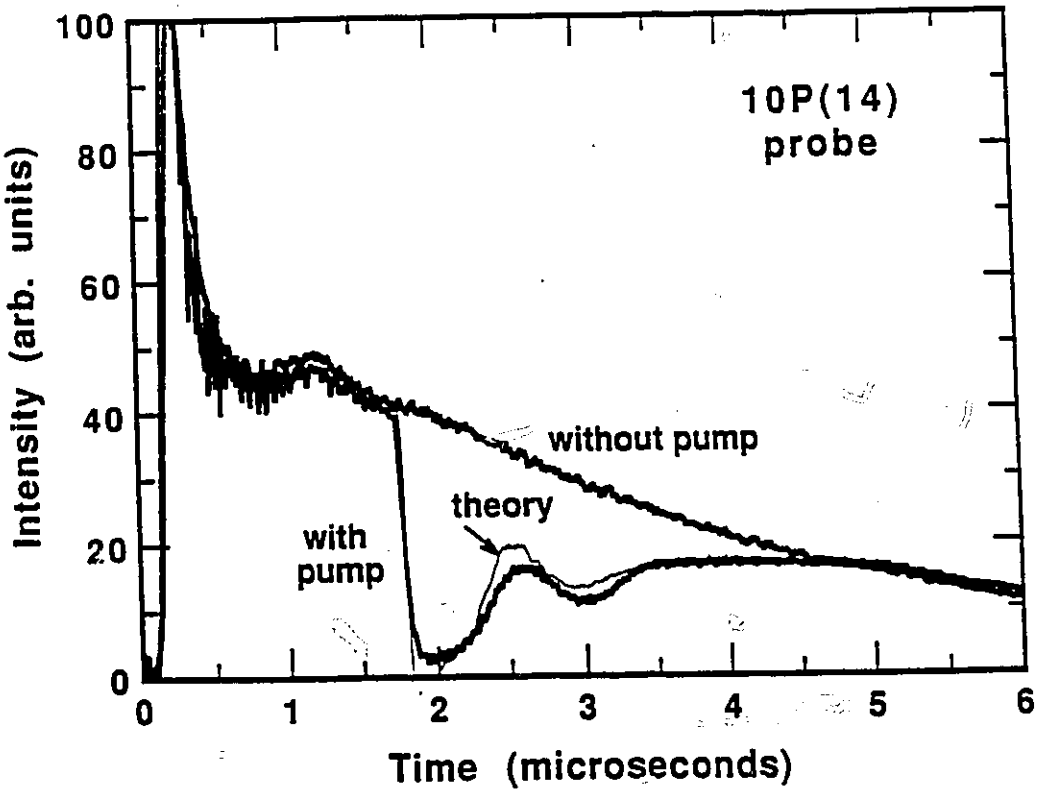


Figure 4.7: Comparison between theory and experiment for the attenuation of a 10P(14) $CO_2$ probe pulse. The concentration is 0.07% $NH_3$ in 5.33 atm of $N_2$ at 200 K. The peak pump intensity is 8.4 MW/cm$^2$ at the input to the 88 cm cell

10P(14) the pump-induced absorption was so strong that there was minimal transmission of the probe - hence the larger error bounds. Once again reasonable agreement is seen between experiment ahd theory at the peak of the pulses for this region dominated by $2\nu_2 \leftarrow 1\nu_2$ absorptions.

### 4.4 Discussion and Conclusions

The results shown in Figs 4.4 to 4.8 demonstrate that good agreement exists between calculations and measurements at the peak of the 9R(30) pump pulse for $CO_2$ probe frequencies varying from 925 - 955 cm$^{-1}$ (10P(8) to 10P(38)). Reasonable

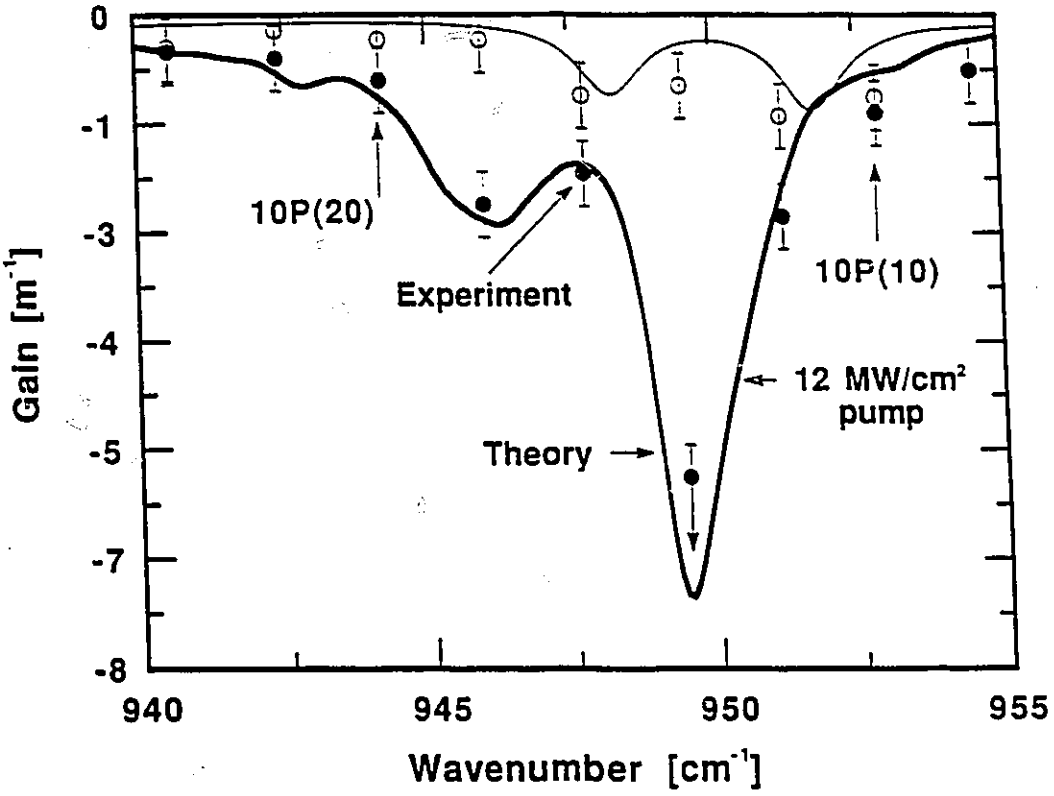


Figure 4.8: Comparison of theory and experiment for measurements made between 940 and 955 $cm^{-1}$. The theoretical lines are calculated for a concentration of 0.04 % $NH_3$ in 5.3 atm of $N_2$ at 200 K. The upper trace represents absorption with the pump absent, and the lower trace shows the absorption at the peak of the 12 $MW/cm^2$ 9R(30) pump pulse. The experimental points are determined by scanning the $CO_2$ probe laser from 10P(22) to 10P(8)

temporal agreement is also seen for the two $CO_2$ probe transitions illustrated in Figs. 4.5 and 4.7. Similar agreement between theory and experiment was found over a wide range of concentrations (0.01 - 0.1 % $NH_3$), pressure (1 - 10 atm), temperature (200 K and 300 K) and for both argon and nitrogen buffer gases. These results confirm that the rate equation model can predict the operation of the high pressure $NH_3$ amplifier over a wide range of conditions.

The experimental measurements shown in Figs 4.5 to 4.8 were all made at dry ice temperatures. The amplifier was cooled to 200 K because theory predicts, and

experiments confirm that significantly better performance is obtained at this temperature than at room temperature. This increased performance is due to the larger pressure broadening coefficient, slower VT,R relaxation rates, and more favourable partition function at lower temperatures. For example, to achieve a 4 $cm^{-1}$ bandwidth with a 2.8 %/cm gain requires a 9 $MW/cm^2$ pump at 200 K and a 29 $MW/cm^2$ pump at 300 K. The inferior amplifier performance at 300 K demonstrates that a high pressure $NH_3$ amplifier should be operated at 200 K. [Little benefit is obtained by lowering the temperature much below 200 K, as the $NH_3$ begins to freeze out at 175 K.]

Having verified the model it is interesting to examine the behaviour of the amplifier under more extreme conditions. Experimentally, with increased concentration (0.12 % $NH_3$) and pump intensity (25 $MW/cm^2$), single pass gains of 150 (5.7 %/cm) were observed at 6.33 atm in agreement with the predictions of the model. This performance is comparable to the best obtainable in $CO_2$ discharge modules without the problems associated with high pressure electrical discharges.

With the present apparatus, the $CO_2$ laser output power limits the investigator to a peak pump intensity of ~25 $MW/cm^2$ (~3 $J/cm^2$ for the pulses shown in Fig. 4.3). If the flux density is increased to 5 $J/cm^2$ for the pulses shown in Fig. 4.3, it should be possible to pump with peak intensities of 40 $MW/cm^2$. The model predicts single pass gains in excess of 69 dB at 6 atm are achievable under these pumping conditions - significantly better performance than that attainable with high pressure $CO_2$ discharges. A further improvement in $NH_3$ amplifier performance can be obtained by pumping with shorter $CO_2$ pump pulses. Preliminary model calculations indicate that a 3 $J/cm^2$ pump pulse with a FWHM of 10 nanoseconds incident upon an optimised $NH_3$ amplifier will produce a single pass gain of 61 dB on the 10P(34) $CO_2$ transition at a pressure of 20 atm.

These results and calculations show clearly that optically pumped $NH_3$ is a viable alternative to discharge-excited $CO_2$ as high pressure amplifier for $CO_2$ radiation, offering both high gain and large bandwidth.

# Chapter 5

# The Hot-Band Laser

## 5.0 Introduction

Chapters 2 through 4 have shown that ammonia is a highly efficient amplifier and oscillator in the 10 to 14 $\mu$m wavelength region on $1\nu_2 \leftarrow$ gs transitions. Lasing action has also been observed on $2\nu_2 \leftarrow 1\nu_2$ transitions of ammonia. The radiation emitted from these transitions is in the 15 - 22 $\mu$m region [1,41,42,43]. Since the completion of this initial work in 1984 much more has been learned about $NH_3$ laser dynamics. In particular, the measurements of Dubé [24,44], and the work described in this thesis enable one to develop a much better model of the $2\nu_2$ hot-band laser than was possible in 1984. In this chapter, lasing action on these $2\nu_2$ transitions is studied, and the rate-equation approach of the previous chapters is extended to consider time-dependent two-step optical pumping of the $2\nu_2$ vibrational level. Preliminary experimental measurements taken at both 200 K and 300 K serve to test the model and to identify its limitations. The model and underlying theory are presented in Sect. 5.1. Section 5.2 discusses the experimental setup and Sect. 5.3 presents the experimental results.

## 5.1 Theory

In order to achieve line-tunable lasing on $2\nu_2 \leftarrow 1\nu_2$ transitions, inversion between relative rotational levels of the $1\nu_2$ and $2\nu_2$ vibrational levels must be achieved, and sufficient population must be present in the lasing levels. As shown in Fig. 5.1, inversion is achieved by transferring population from the $1\nu_2$s level to the $2\nu_2$a vibrational level of ammonia. This transfer is accomplished by pumping the

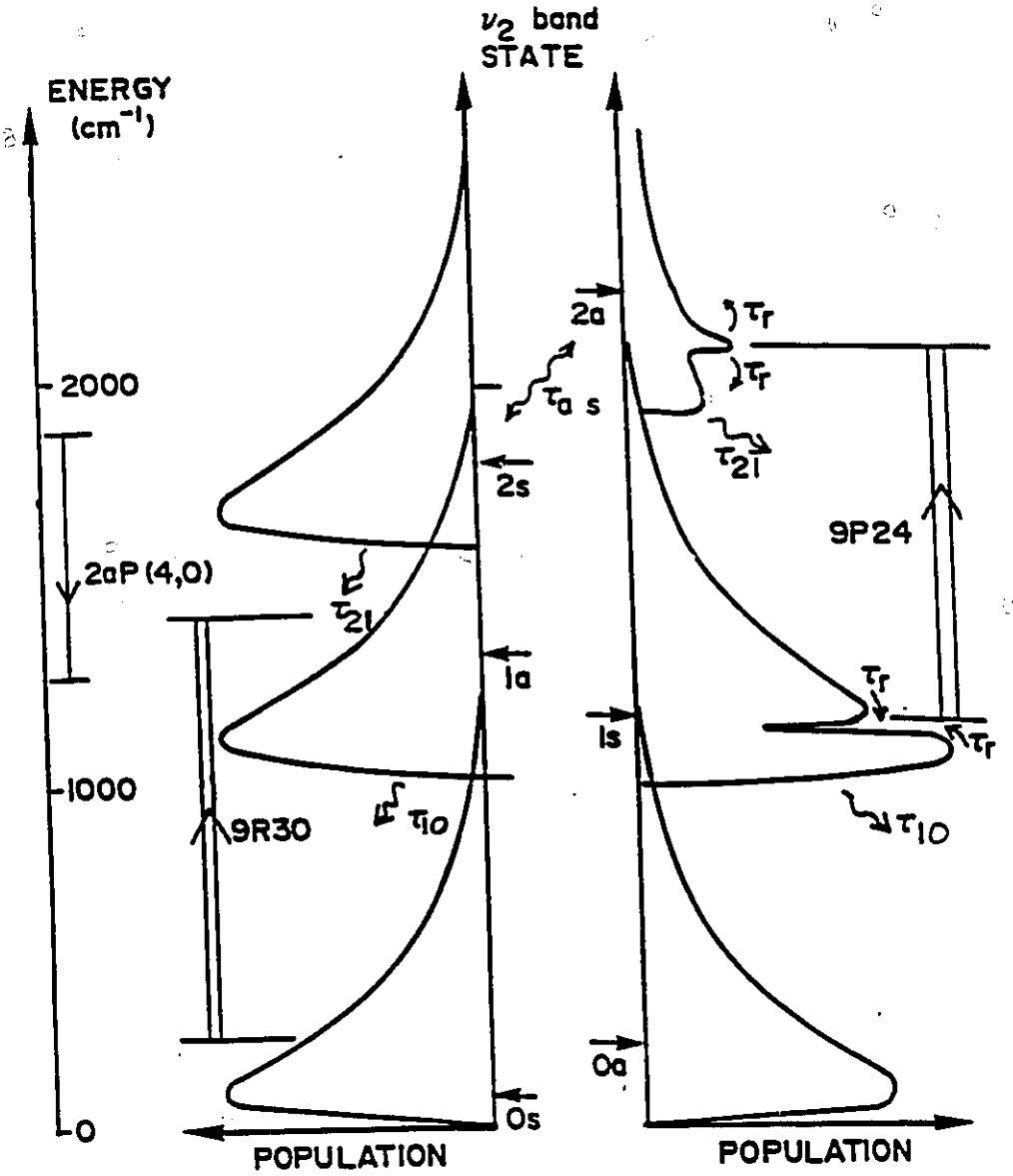


Figure 5.1: Energy levels of $NH_3$ relevant to $2\nu_2$ laser operation. The $CO_2$ 9R(30) pump transfers population from the ground state to the $1\nu_2$ vibrational level. The $CO_2$ 9P(24) pulse moves population from the $1\nu_2$ state to the antisymmetric $2\nu_2$ state. $\tau_r$ is the characteristic time for the redistribution of population within a vibrational state, and $\tau_{as}$ is the characteristic time for the rate of conversion between the $2\nu_2$ symmetric and antisymmetric states. VT,R relaxation dominates the vibrational level decay and is denoted by $\tau_{10}$ and $\tau_{20}$

2sR(4,3) transition in $NH_3$ by the $CO_2$ 9P(24) laser transition. Rapid rotational relaxation and transfer between a and s symmetries of ammonia serve to quickly redistribute the population from the pumped rotational state to the entire rotational manifold and to repopulate the lower pumped state. Since there is a large separation of the $2\nu_2$a and $2\nu_2$s states (cf Fig 5.1), pumping on an s-branch transition has the potential to create inversion on all a-branch transitions - P, Q, or R.

As the thermal population in the $1\nu_2$ vibrational level is small, this population is increased by pumping sR(5,K) with $CO_2$ 9R(30) laser radiation. The 9R(30) pump effectively increases the thermal population of the $1\nu_2$ "ground state" by more than an order of magnitude.

In contrast to the operation of the conventional $NH_3$ system, in which perturbations to the rotational populations played only a secondary effect in the gain dynamics, rotational level dynamics dominate the operation of the $2\nu_2$ system. Rotational levels affected by the $2\nu_2 \leftarrow 1\nu_2$ pump field experience a perturbation as large as a factor of two or more from the thermalized value (cf 10% in $1\nu_2$ case). This difference stems from the fact that the VT,R relaxation rate for the $2\nu_2$ level is an order of magnitude faster than the $1\nu_2$ rate while the rotational relaxation rate is approximately the same for both levels. The net effect of this on the $2\nu_2$ laser is that the rotational relaxation rate out of the upper ($2\nu_2$) rotational level limits the rate of pumping, the level of vibrational inversion, and hence the maximum efficiency attainable.

A rate equation model has been developed to take into account these effects and to describe gain in optically pumped $2\nu_2$ $NH_3$ lasers. The model evaluates changes in level populations based on three main assumptions:

1. those rotational populations which are not interacting with a radiation field are always thermalized

2. the ortho- and para- species of $NH_3$ are treated as two independent species

3. a and s symmetries of $NH_3$ are in thermal equilibrium for the ground state and $1\nu_2$ vibrational level.

Assumption 1 is justified as the rotational relaxation rate in dilute $NH_3$ is still two orders of magnitude faster than the V-T relaxation rate [18,24] and thus the population distribution remains close to thermal equilibrium in those levels not directly coupled to a radiation field. Assumption 2 is justified as recent direct measurements of collisional relaxation rates have shown that the rate of vibrational energy transfer between ortho- and para- $NH_3$ is very slow [26]. Assumption 3 is validated by the measurements of Dubé [24] in which the relaxation rates of the $2\nu_2$s and $2\nu_2$a vibrational levels were seen to be the same when 2sR(4,3) was pumped. Dubé concludes that the rate at which $2\nu_2$s and $2\nu_2$a levels approach thermal equilibrium is an order of magnitude faster than the $2\nu_2$ decay rate [44]. As this rate is fast compared to the $1\nu_2$ relaxation rate, it can be neglected in dealing with the ground state and first vibrational level. It is, however, necessary to take this rate into account when one looks at the $2\nu_2$ vibrational level.

A computer model has been developed based on these assumptions and used to calculate the gain in both cw and pulsed $NH_3$ systems. Although changes in the pump pulse intensity are slow relative to the VT,R relaxation rate of the $2\nu_2$ level, they are fast relative to the VT,R relaxation rate of the $1\nu_2$ level, under the experimental conditions described later in this chapter. Thus a time dependent model is necessary to understand the present experiments, in contrast to the quasi-cw treatment possible for the low pressure $1\nu_2$ laser used in Chapter 2. In the model the total $NH_3$ population is assumed to lie in the ground state and the first two excited states of the $\nu_2$ mode.

The vibrational levels are treated as anharmonic with the actual energy levels used in all calculations. As all pump and emission transitions of interest occur in the ground and first two $\nu_2$ vibrational states, the equations are written chiefly in terms of $N_0$, $N_1$, and $N_2$, the populations of the ground state and lowest two vibrational levels. The total population is the sum of the $N_0$, $N_1$, and $N_2$.

In general, four terms need to be included in determining the variation of the rotational level populations with time. The first term represents the tendency of the perturbed rotational level population to approach thermal equilibrium with the other rotational levels in the same vibrational state. The second term is the population change due to absorption or stimulated emission. The third term represents population lost due to decay to all the rotational levels to a lower vibrational state, while the final term represents the population gained due to molecules decaying from a higher vibrational state.

The complete model equations for $N_0$, $N_1$, $N_2$, and the rotational levels that interact with radiation fields are:

$$\frac{dN_0}{dt} = \frac{N_1 - A \times N_0}{\tau_{10}} - P_1 - P_2 \tag{5.1}$$

$$\frac{dN_1}{dt} = \frac{N_2 - B \times N_1}{\tau_{21}} - \frac{N_1 - A \times N_0}{\tau_{10}} + P_1 + P_2 - P_3 - P_4 \tag{5.2}$$

$$\frac{dN_{2a}}{dt} = -\frac{N_{2a} - B_a \times N_1}{\tau_{21}} - \frac{N_{2a} - B_{aa} \times N_{2s}}{\tau_{aa}} + P_3 \tag{5.3}$$

$$\frac{dN_{2s}}{dt} = -\frac{N_{2s}-B_s\times N_1}{\tau_{21}} + \frac{N_{2s}-B_{as}\times N_{2s}}{\tau_{as}} + P_4 \qquad (5.4)$$

$$\frac{dr_a}{dt} = -\frac{r_a-r_a^e}{\tau_r} - P_1 + \frac{f_a N_1 - A\times r_a}{\tau_{10}} \qquad (5.5)$$

$$\frac{dr_b}{dt} = -\frac{r_b-r_b^e}{\tau_r} + P_1 - \frac{r_b-A\times N_0 f_b}{\tau_{10}} + \frac{f_b N_2 - B\times r_b}{\tau_{21}} \qquad (5.6)$$

$$\frac{dr_c}{dt} = -\frac{r_c-r_c^e}{\tau_r} - P_2 + \frac{f_c N_1 - A\times r_c}{\tau_{10}} \qquad (5.7)$$

$$\frac{dr_d}{dt} = -\frac{r_d-r_d^e}{\tau_r} + P_2 - \frac{r_d-A\times N_0 f_d}{\tau_{10}} + \frac{f_d N_2 - B\times r_d}{\tau_{21}} \qquad (5.8)$$

$$\frac{dr_e}{dt} = -\frac{r_e-r_e^e}{\tau_r} - P_3 - \frac{r_e-A\times N_0 f_e}{\tau_{10}} + \frac{f_e N_2 - B\times r_e}{\tau_{21}} \qquad (5.9)$$

$$\frac{dr_f}{dt} = -\frac{r_f-r_f^e}{\tau_r} + P_3 - \frac{r_f-B_a\times N_1 f_f^a}{\tau_{21}} - \frac{r_f-B_{as}\times N_{2s} f_f^a}{\tau_{as}} \qquad (5.10)$$

$$\frac{dr_g}{dt} = -\frac{r_g - r_g^e}{\tau_r} - P_4 - \frac{r_g - A \times N_0 f_g}{\tau_{10}} + \frac{f_g N_2 - B \times r_g}{\tau_{21}} \qquad (5.11)$$

$$\frac{dr_h}{dt} = -\frac{r_h - r_h^e}{\tau_r} + P_4 - \frac{r_h - B_s \times N_1 f_h^s}{\tau_{21}} + \frac{f_h^s N_{2a} - B_{as} \times r_h}{\tau_{as}} \qquad (5.12)$$

and

$$N = N_0 + N_1 + N_2$$

Throughout this chapter $r_a$ denotes the 0s(5,0) level, $r_b$ the 1a(6,0) level, $r_c$ the 0s(5,3) level, $r_d$ the 1a(6,3) level, $r_e$ the 1s(4,3) level, $r_f$ the 2a(5,3) level and $r_g$ and $r_h$ the lower and upper levels of the lasing transition--assumed an a-transition. A, B, $B_a$, $B_s$, $B_{as}$, and $f_i$ are the thermal equilibrium ratios - $N_1^e/N_0^e$, $N_2^e/N_1^e$, $N_{2a}^e/N_1^e$, $N_{2s}^e/N_1^e$, $N_{2a}^e/N_{2s}^e$, $r_i^e/N_i^e$ respectively. The pumping terms, due to the radiation fields present in the cavity are defined as follows: $P_1$ and $P_2$ are the rates of optical pumping of molecules to the first vibrational level from the ground state through the two transitions (sR(5,0) and sR(5,3)) interacting with the 9R(30) pump; $P_3$ is the rate of optical pumping of molecules to the second vibrational level due to 9P(24); and $P_4$ is the rate of removal of molecules from the second vibrational level due to stimulated emission. $\tau_{10}$ is the VT,R relaxation rate for the $1\nu_2$ vibrational state to the ground state, $\tau_{21}$ is the $2\nu_2 \leftarrow 1\nu_2$ VT,R relaxation rate, $\tau_{as}$ is the $2\nu_2$a $\leftarrow 2\nu_2$s VT,R relaxation rate, and $\tau_r$ is the rotation relaxation rate defined by:

$$\tau_r = (2\pi K \Delta\nu)^{-1} \qquad (5.13)$$

As in chapter 2, K is a phenomenological constant introduced into the model to account for the fact that all phase changing collisions (collisions that contribute to the linewidth) do not serve to redistribute population in the rotational manifold.*

The rate equations are solved for the final populations using a time dependent, finite difference approach. From the final populations the absorption or gain on the transitions of interest are calculated (for small signal gain, $P_4$ is set equal to zero) Tables 4.1 and 5.1 list the molecular constants used in the model. $\tau_{as}$ is set equal to $\tau_{21}/10$.

Table 5.1: $2\nu_2$ VT,R Relaxation rates [$\mu s^{-1}$ $Torr^{-1}$] [a]

| Collision Partner | Temperature | |
|---|---|---|
| | 200 K | 300 K |
| $NH_3$ | 4.4 [b] | 5.6 [c] |
| Ar | 0.034 [b] | 0.046 [c] |
| $N_2$ | 0.059 [b] | 0.1 [c] |

[a] the rate of change between the symmetric and asymmetric $2\nu_2$ states is set equal to 10 times the $2\nu_2$ VT,R relaxation rate

[b] estimated using:

$$k_{VT_2}(200\ K) = k_{VT_2}(300\ K) \times \frac{k_{VT_1}(200\ K)}{k_{VT_1}(300\ K)}$$

[c] Dubé and Reid [ref. 24]

* As no direct small signal gain measurements were taken, it is difficult to determine the exact value of K. It appears that for the ground state and $1\nu_2$ vibrational levels that $K_0 = K_1 \sim 0.5$ (as determined in chapter 2) while for the $2\nu_2$ vibrational level calculations indicate that $K_2 \sim 0.1 \rightarrow 0.3$.

In the experiments described in this chapter, there is very little variation in the intensity of the 9P(24) pump along the length of the oscillator. However, in some experiments the intensity of the 9R(30) pump beam varies significantly along the length. This variation is due to two factors:

1. 9R(30) experiences para as well as ortho absorption

2. a very low intensity 9R(30) pump was used in some experiments.

In the case of significant 9R(30) attenuation, it is necessary to split the oscillator cell into small sections and calculate the stimulated emission and pump absorption separately for each section.

Figure 5.2 illustrates the results of model calculations carried out at 300 K. The conditions chosen are similar to the actual experimental conditions.

**5.2 Experimental Apparatus**

Figure 5.3 is a schematic diagram of the apparatus. Two TEA $CO_2$ lasers are used to pump the oscillator. The first laser operates on the 9R(30) transition at 1084.635 $cm^{-1}$. The output pulse is typically a few microseconds long with a total energy of 2 Joules. The second $CO_2$ laser operates on the 9P(24) transition at 1043.163 $cm^{-1}$. Its output pulse is typically 5 $\mu$s long with a total energy of 6 J. The $NH_3$ oscillator is comprised of an 0.88 m long pyrex gas cell sealed with CdTe Brewster windows. The oscillator cell is longitudinally pumped by the internal reflection off the Brewster angle windows. Inlet and outlet valves allow the gas mixture to be flowed continuously and, hence, the $NH_3$ concentration to be easily varied. The $NH_3$ cavity was formed by two concave copper mirrors. $NH_3$ radiation reflected from one

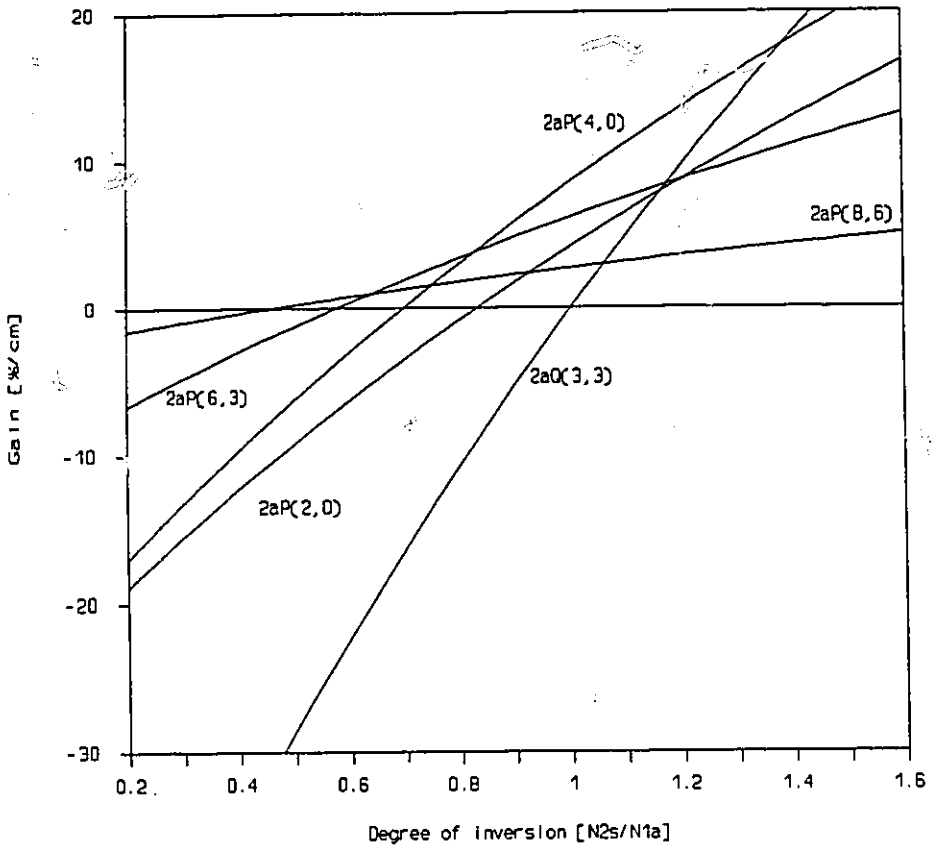


| Intensity [kW/cm$^2$] | 50 | 100 | 150 | 300 | 700 | 1000 | 10000 |
|---|---|---|---|---|---|---|---|
| Inversion [$N_2s/N_1a$] | 0.72 | 0.88 | 0.97 | 1.06 | 1.13 | 1.15 | 1.18 |

Figure 5.2: Calculated inversion ratio and small-signal gain on $2\nu_2 \leftarrow 1\nu_2$ transitions as a function of 9P(24) pump intensity. The calculation is carried out for a mixture of 0.75 % $NH_3$ in 100 Torr Ar at 300 K. The 9R(30) pump intensity is held fixed at 10 kW/cm$^2$ (corresponding to an inversion ratio of $N_1/N_0$ = 0.12). 50% of phase changing collisions are assumed to redistribute population in the ground state and $1\nu_2$ vibrational level. The corresponding figure for the $2\nu_2$ vibrational level is 10%. The figure illustrates the variation of small signal gain with inversion ($N_2s/N_1a$), while the table below shows the relationship between the 9P(24) pump intensity and the inversion

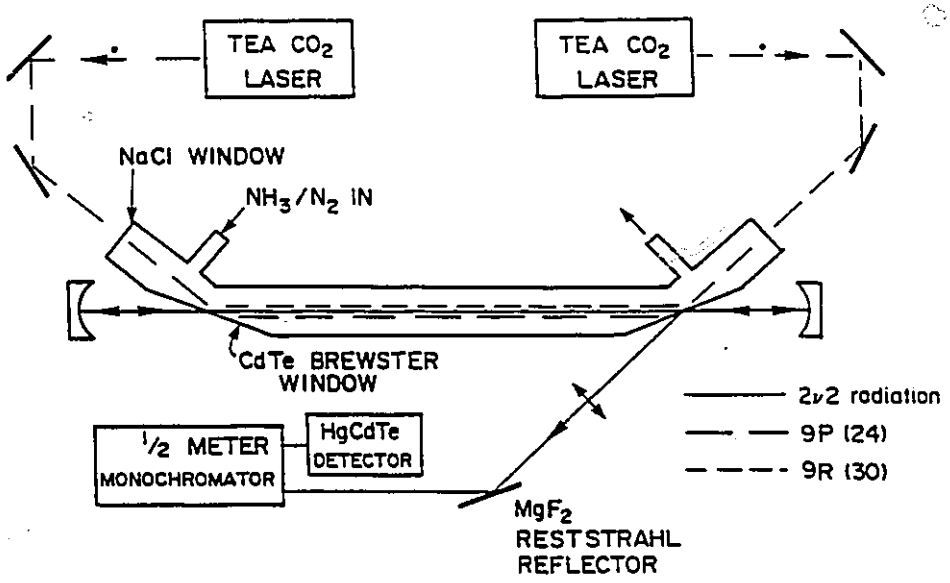


Figure 5.3: Schematic diagram of the $2\nu_2$ laser. A detailed description of the optics can be found in the text

of the CdTe Brewster windows was Reststrahl* reflected off a piece of $MgF_2$ and focused through a 0.5 m monochromator onto a HgCdTe detector. Typical traces of the incavity pump profiles are shown in Figs. 5.4 and 5.5.

### 5.3 Experimental Results

*A. At 300 K*

Table 5.2 summarizes the lines on which lasing was observed. These lines are the same as those observed by Morrison [43] with the addition of the 2aP(9,3) transition. Two lines observed by Morrison to lase intermittently, 2aQ(3,3) and

* Reststrahlen reflection peaks occur when the absorption coefficient is very high and the refractive index changes sharply. High reflectivity is thus the result of a resonance between the incident radiation and the natural vibration frequency of the lattice ions. The Reststrahl reflection in $MgF_2$ serves to effectively separate the pump radiation from the $2\nu_2$ hot-band lasing.

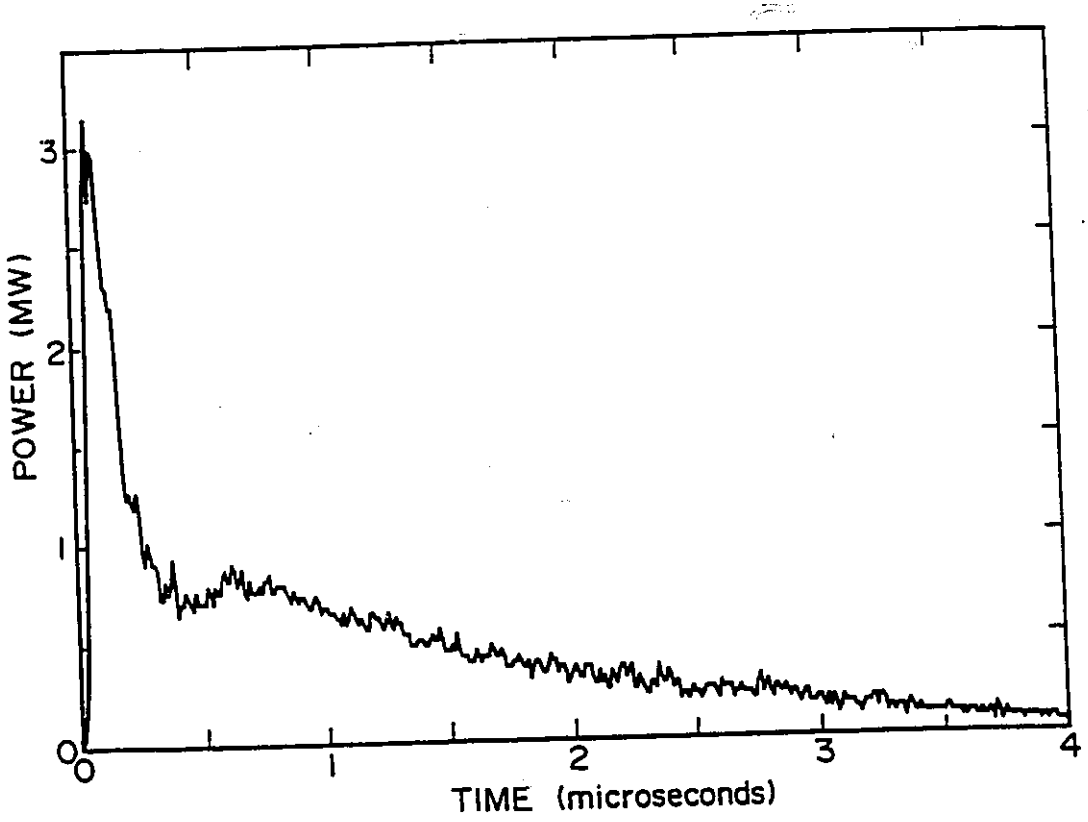


Figure 5.4: Typical 9P(24) pump pulse shape recorded by the digital oscilloscope. At the entrance of the laser, the total energy per pulse is 1.9 J ± 10% in a 2.5 ± 0.5 $cm^2$ area

2aP(2,0), were not observed.

Although no small signal gain measurements were made, one can estimate both the level of inversion (N2s/N1a) and the absolute gain. The lines on which lasing is observed serve to determine the level of inversion (N2s/N1a), as the variation of gain with inversion differs from transition to transition. For example, as seen in Fig. 5.2, at levels of inversion below 1.1, 2aQ(3,3) will not lase no matter how much population is transferred to the $1\nu_2$ ground state. As lasing could not be obtained on 2aQ(3,3), this strongly suggests that the level of inversion is below 1.1. On the other hand, for inversion levels less than 0.83, gain is higher on 2aP(6,3) than on 2aP(4,0) (cf Fig.

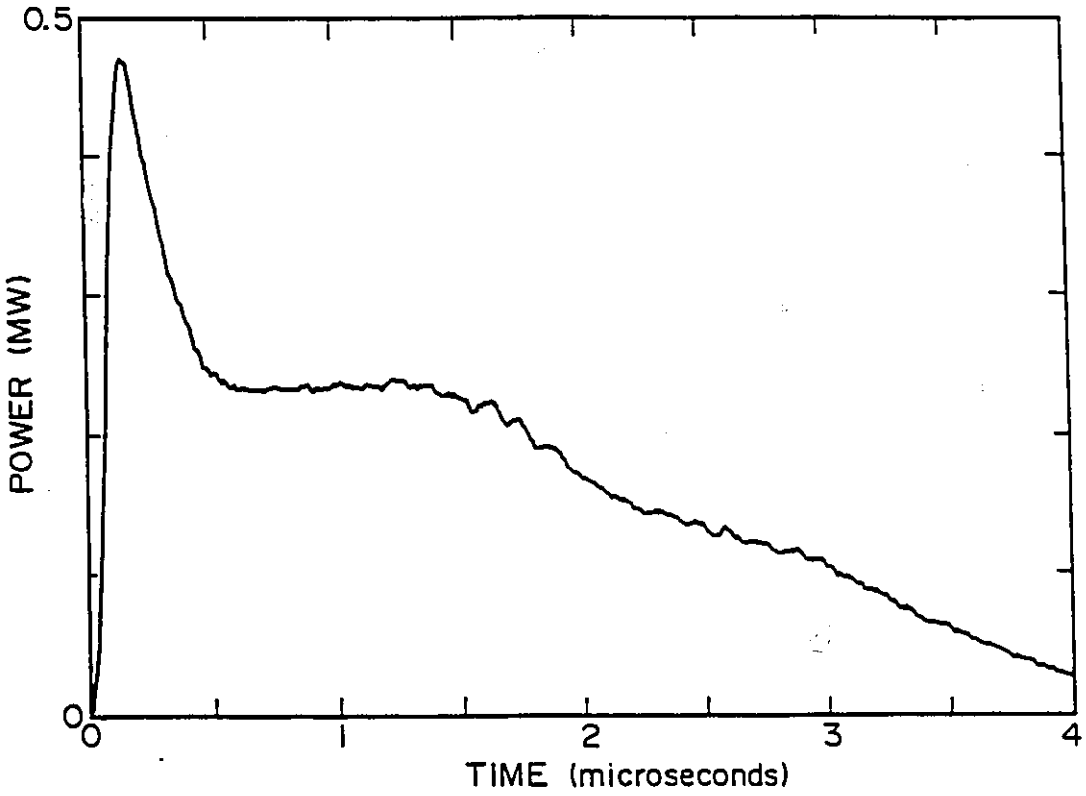


Figure 5.5: Typical 9R(30) pump pulse shape recorded by the digital oscilloscope. The total energy of the pulse at the entrance of the laser cavity is 700 mJ ± 10% in a 2.5 ± 0.5 $cm^2$ area

5.2). Although under most experimental conditions both lines were observed to lase, the delay before lasing on 2aP(4,0) was less than that on 2aP(6,3). As the buildup time to lasing is inversely proportional to gain, it follows that gain is higher on 2aP(4,0) and thus the inversion level is greater than 0.83.

Summarizing the previous paragraphs, the typical inversion achieved in experiments was between 0.83 and 1.1.

By choosing the appropriate value of $K_2$, the inversion ratio $N_2a/N_2s$ predicted by the model can be made to agree with the experimental value as determined by the relative gain on the different transitions. Generally, a value of $K_2$ in the range of 0.1

Table 5.2: Summary of $2\nu_2$ transitions observed at 300 K

| Transition | Wavenumber [$cm^{-1}$] | Experimental Conditions [a] |
|---|---|---|
| 2aP(4,0) | 554.11 | 0.08% $NH_3$ in ~110 Torr $N_2$, ~10 Torr Ar |
| 2aP(4,3) | 549.23 | 0.15% $NH_3$ in ~100 Torr $N_2$, ~20 Torr Ar |
| 2aP(5,3) | 531.98 | 0.08% $NH_3$ in ~110 Torr $N_2$, ~10 Torr Ar |
| 2aP(6,3) | 515.44 | 0.08% $NH_3$ in ~110 Torr $N_2$, ~10 Torr Ar |
| 2aP(7,3) | 499.76 | 0.08% $NH_3$ in ~110 Torr $N_2$, ~10 Torr Ar |
| 2aP(8,0) | 491.10 | 0.33% $NH_3$ in ~70 Torr $N_2$, ~50 Torr Ar |
| 2aP(7,6) | 485.37 | 0.33% $NH_3$ in ~70 Torr $N_2$, ~50 Torr Ar |
| 2aP(8,3) [b] | 484.97 | 0.33% $NH_3$ in ~70 Torr $N_2$, ~50 Torr Ar |
| 2aP(9,3) [b,c] | 471.08 | 0.47% $NH_3$ in ~50 Torr $N_2$, ~70 Torr Ar |
| 2aP(8,6) [b] | 468.87 | 0.47% $NH_3$ in ~50 Torr $N_2$, ~70 Torr Ar |

[a] Total pressure ~ 120 ± 20 Torr, conditions recorded are minimum concentration at which lasing was observed
[b] required a higher 9P(24) pump intensity
[c] output not stable

to 0.3 is required to obtain agreement between experiment and calculations. A further check on the validity of the model can be provided by estimating the absolute value of the gain to obtain lasing.

No direct measurements of gain coefficients have been made in the present apparatus, but one can estimate the peak gain coefficients from the measured delay

time to lasing and the estimated cavity losses. This type of estimate is more accurate when the laser is operating near threshold with long delay times to lasing. For example, in a mixture of 0.745% $NH_3$ in 58 Torr of Ar pumped by 1.9 J of 9P(24) (Fig. 5.3), no lasing was observed without 9R(30). Theoretical calculations suggest that a gain of 14 %/m is present in the cavity. As estimates of the gain required for lasing are close to this value, it is not surprising that it does not lase. When a small amount (~20 mJ) of 9R(30) was introduced into the cell, lasing was detected delayed 2 $\mu$s relative to the 9P(24) pump pulse. This is expected as model calculations indicate that even such a small amount of 9R(30) can significantly increase small-signal gain. Reasonable agreement is thus seen between model calculations and these preliminary experimental results at 300 K. The 200 K results are discussed in the following section.

*B. At 200 K*

The experiments were repeated at 200 K. Table 5.3 summarizes the results at 200 K. Higher levels of inversion were achieved in agreement with the model predictions. However, at 200 K one surprising result was obtained: lasing was observed on a number of transitions (cf Table 5.3) in the absence of any 9R(30) pump. For example, 2aP(6,3) was observed to lase in a mixture of 0.745% $NH_3$ in 194 Torr of Ar; conditions under which 2aQ(3,3) did not lase. With reference to Fig. 5.6, one can see that this suggests that the level of inversion is < 1.2. For this level of inversion, the model predicts that the gain on 2aP(6,3) is only ~ 50% of the small signal gain required for lasing. Similar anomalously high gain is observed on 2aP(4,0). For a 0.745% mixture of $NH_3$ in 120 Torr of Ar, lasing was observed with a time delay of 1$\mu$s relative to the start of the 9P(24) pump pulse. This experimental observation requires a minimum small-signal gain of 24 %/m -- approximately twice

Table 5.3: Summary of $2\nu_2$ transitions observed at 200 K

| Transition | Wavenumber [$cm^{-1}$] |
|---|---|
| 2aQ(3,3) [a] | 628.26 |
| 2aP(2,0) [a] | 590.34 |
| 2aP(4,0) [a] | 554.11 |
| 2aP(4,3) [a] | 549.23 |
| 2aP(5,3) [a] | 531.98 |
| 2aP(6,3) [a] | 515.44 |
| 2aP(7,3) [a] | 499.76 |
| 2aP(8,0) | 491.10 |
| 2aP(7,6) | 485.37 |
| 2aP(8,3) | 484.97 |

[a] lases without any 9R(30) pump

the 12 %/m predicted by theory. Clearly further investigation is required to understand fully the behaviour at 200 K. Nevertheless, the initial results are very encouraging - it is not often that experiment works better than theory.

Despite the absence of a quantitative explanation of this effect, it is interesting to speculate on the mechanism of lasing at 200 K in the absence of 9R(30) pumping. Figure 5.7 shows a comparison of lasing with and without the 9R(30) pump present. The 9R(30) pump serves to transfer population rapidly to the $1\nu_2$ level creating a higher small signal gain and thus a very short delay time until lasing. When the 9R(30) is absent, inversion is quickly obtained on the $2\nu_2 \leftarrow 1\nu_2$ transitions but since there is little population in these levels under thermal conditions, lasing does not occur. However, the depletion of the $1\nu_2$ level lowers the ratio of the $1\nu_2$ vibrational level to ground state population below the thermal equilibrium value. Thus the VT,R

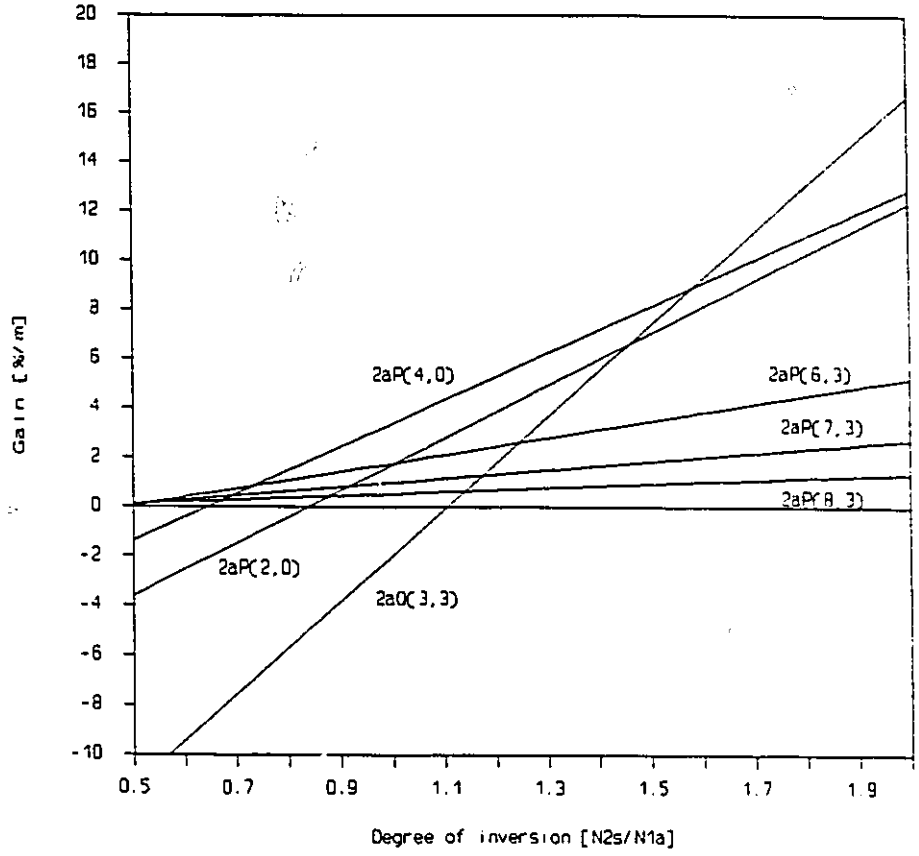


| Intensity [kW/cm$^2$] | 25 | 50 | 100 | 150 | 300 | 700 | 1000 |
|---|---|---|---|---|---|---|---|
| Inversion [$N_2s/N_1a$] | 1.1 | 1.5 | 1.8 | 2.0 | 2.2 | 2.3 | 2.4 |

Figure 5.6: Repeat of Fig. 5.2 at a temperature of 200 K in the absence of the 9R(30) pump

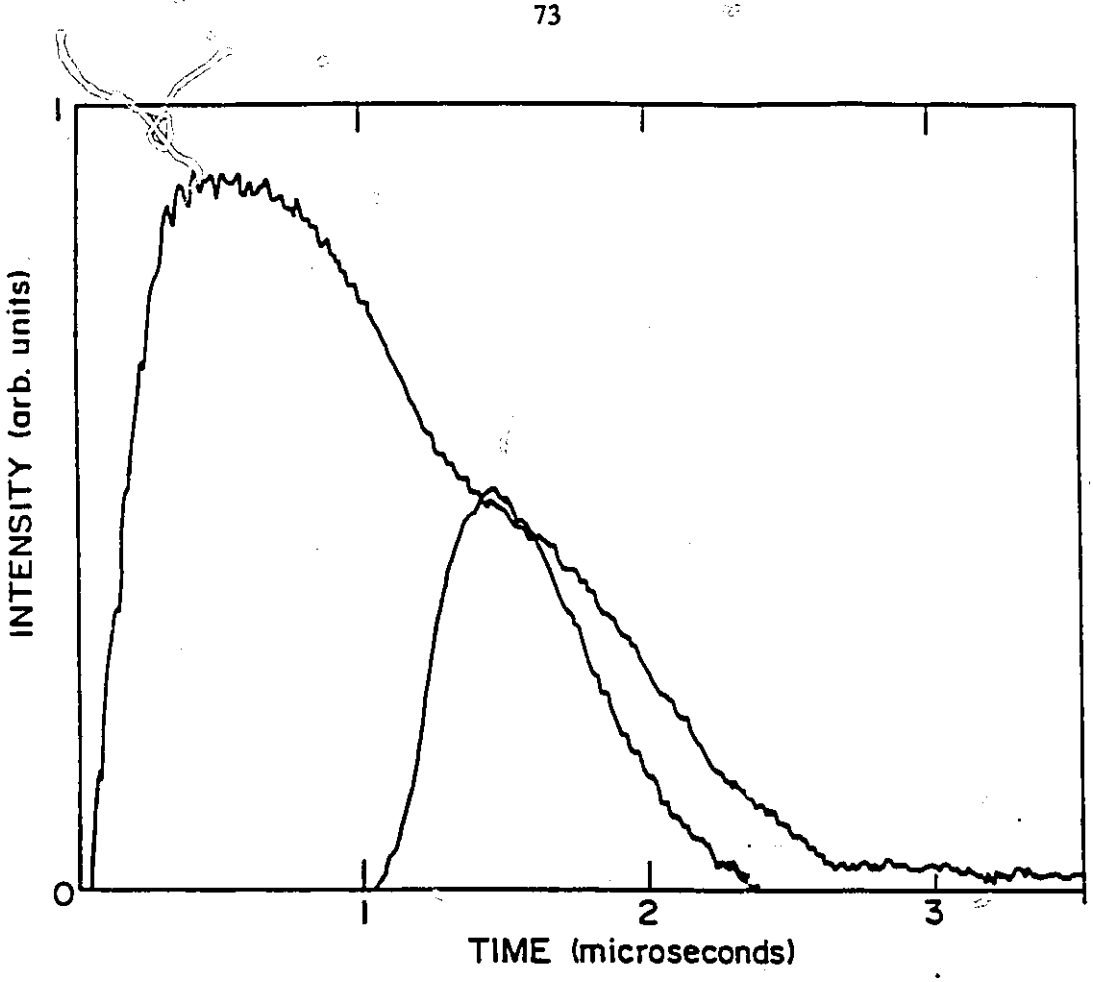


Figure 5.7: Comparison of 2aP(4,0) laser output with and without the 9R(30) pump present. The oscillator contains 0.775% $NH_3$ in 120 Torr of Ar at 200 K. 1.9 J of 9P(24) pump is incident on the oscillator. Lasing is delayed 100 ns when the oscillator is pumped by 9R(30). Without 9R(30), the delay is increased to 1.1 $\mu$s

relaxation process acts as a pump transferring population *up* from the ground state to the first vibrational level. This additional population increases the gain on the $2\nu_2 \leftarrow 1\nu_2$ transitions allowing lasing to occur. Under the experimental conditions used here, this transfer takes place on a time scale of approximately 1 to 2 $\mu$s.

One way of increasing the $1\nu_2$ VT,R "pumping" rate is to increase pressure. As shown in Fig. 5.8, the result of increasing the VT,R pumping rate is to decrease the required buildup time, i.e., small signal gain is increased.

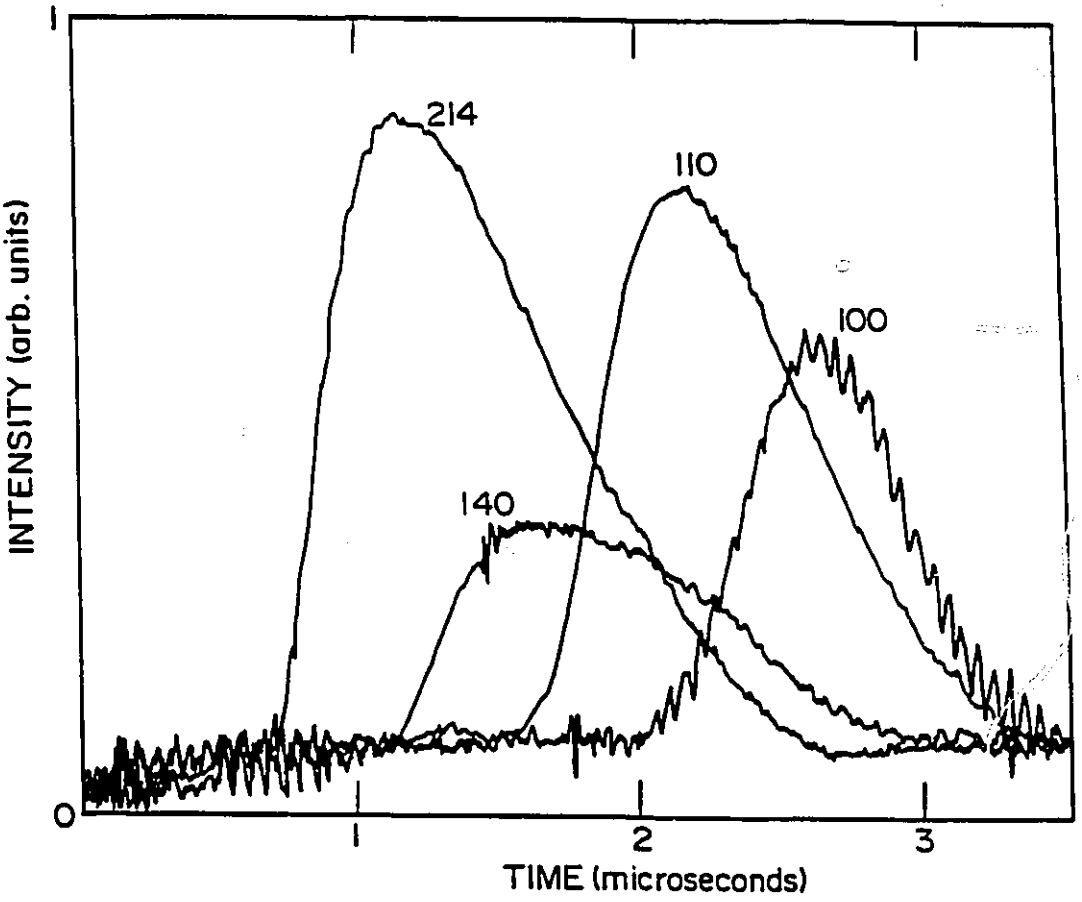


Figure 5.8: Comparison of 2aP(4,0) laser output at a number of pressures in the absence of the 9R(30) pump. The time scale is relative to the incidence of the 9P(24) pump, and the pressures indicated are in Torr. The oscillator contains 0.3% $NH_3$ in $N_2$ and Ar at 200 K. 1.9 J of 9P(24) is incident on the oscillator (as the vertical scale is not the same for all traces, there is no significance in the variation of pulse heights)

### 5.4 Discussions and Conclusions

A model has been developed to describe the operation of the $2\nu_2$ laser. In order to understand better the operation of this laser system, two further experiments should be carried out. The first experiment - to measure K - would be an oscillator/amplifier experiment. The experimental setup for this could be the same

as that shown in Fig. 2.2 with the $CO_2$ laser operating on the 9P(24) transition and the Au:Ge detector replaced by one sensitive in the 15-21 $\mu$m region. By running the oscillator at 200 K, only one $CO_2$ laser would be required.

The second experiment is designed to check if the $\nu_4$=1a (l=+) state is coupled to the $2\nu_2$s vibrational level.* A $CO_2$ laser operating on 9P(24) would be used to pump the $2\nu_2$ band. A change in population of the $\nu_4$ level would easily be determined by monitoring the transmission of a tunable diode laser probing the 5 $\mu$m $2\nu_4$ <- $1\nu_4$ transition. The experimental setup of Dubé [24] is especially suited for this measurement.

The ability to use only one pump to get laser action, as well as simplifying the oscillator/amplifier experiment, also simplifies the construction of a line-tunable oscillator. The simple experimental setup of Fig. 3.1 could be used to provide grating tunable operation from 10 to 21 $\mu$m, from 10 - 14 $\mu$m on $1\nu_2 \leftarrow$ gs transitions with the $CO_2$ laser tuned to 9R(30) and from 15 - 21 $\mu$m on $2\nu_2 \leftarrow 1\nu_2$ transitions with the $CO_2$ laser tuned to 9P(24).

---

*Some researchers have suggested the possibility that there is a rapid population transfer from the $2\nu_2$s to the $1\nu_4$s ($l$ = +) vibrational level [24]. Urban *et al.* [45] have observed strong mixing at 300 K of the wavefunctions for some of the rotational-vibrational states in the $2\nu_2$s and $1\nu_4$ vibrational levels. For a few high-J states this strong coupling makes it impossible to denote a state as either a $\nu_2$ or $\nu_4$ state. Further support for the possibility of rapid transfer is found in the work of Jacobs [1] who, following two photon excitation of a para $2\nu_2$ level, observed lasing not only on the expected $2\nu_2$ transitions but also on 2 other transitions in the 6 $\mu$m region which they tentatively identified as $\nu_4$ transitions. If one assumes rapid coupling in the model presented in this chapter, one is required to set $K_2$ = 1 and $\tau_{as}$ = 0 to account for the experimental results.

# Chapter 6

## Conclusions

In this thesis a rate equation model approach based on the $NH_3$ molecular dynamics has been shown to describe accurately the operation of oscillators and amplifiers that use a dilute mixture of $NH_3$ in a buffer gas as the active medium. The model has been seen to be valid over a pressure range of 2 orders of magnitude (0.1 atm to 10 atm); a concentration range of 2 orders of magnitude (0.01 to 0.745 % $NH_3$); temperatures from 200 to 300 K; for Ar, $N_2$ and He buffer gases; and for both $1\nu_2 \leftarrow$ gs and $2\nu_2 \leftarrow 1\nu_2$ transitions.

$NH_3$ oscillators and amplifiers have been shown to be highly efficient sources of grating tunable radiation in the 10 - 14 $\mu$m region. Output energies as high as 4.6 J and conversion efficiencies as high as 35% have been observed. In high pressure operation continuous tunability over discrete sections of the spectrum (~4 $cm^{-1}$ in the aQ-branch) has been demonstrated. A model of the $2\nu_2$ hot-band laser has been developed and preliminary experiments completed to test the model. Lasing has been observed on $2\nu_2$ transitions with only the 9P(24) pump present - an unexpectedly good result. Further research is required to understand fully the $2\nu_2$ laser.

## References


1. R. R. Jacobs, D. Prosnitz, W. K. Bischel, and C. K. Rhodes, "Laser generation from 6 to 35 $\mu$m following two-photon excitation of ammonia", *Appl. Phys. Lett.*, 29, 710-712 (1976)

2. D. F. Kroeker and J. Reid, "Line-tunable cw ortho- and para-$NH_3$ lasers operating at wavelengths of 11 to 14 $\mu$m", *Appl. Opt.*, 25, 2929-2933 (1986)

3. Handbook of Laser Science and Technology, Vol. II: Gas Lasers, ed. M.J. Weber (CRC Press, Florida, 1982)

4. B. I. Vasil'ev, A. Z. Grasyuk, A. P. Dyad'kin, A. N. Sukhanov, and A. B. Yastrebkov, "High-power efficient optically pumped $NH_3$ laser, tunable over the range 770-890 $cm^{-1}$", *Sov. J. Quantum Electron.*, 10, 64-68 (1980)

5. P. K. Gupta, A. K. Kar, M. R. Taghizadeh, and R. G. Harrison, "12.8-$\mu$m $NH_3$ laser emission with 40-60% power conversion and up to 28% energy conversion efficiency", *Appl. Phys. Lett.*, 39, 32-34 (1981)

6. R. V. Ambartsumian, A. Z. Grasiuk, A. P. Pyadkin, N. P. Furzikov, V. S. Letokhov, and B. I. Vasil'ev, "Isotopically Selective Dissociation of $CCl_4$ Molecules by $NH_3$ Laser Radiation", *Appl. Phys.*, 15, 27-30 (1978)

7. J. J. Tiee and C. Wittig, "Isotopically selective ir photodissociation of $SeF_6$", *Appl. Phys. Lett.*, 32, 236-238 (1978)

8. F. Magnotta and I. P. Herman, "Infrared laser multiple-photon dissociation of $CTCl_3$: Wavelength dependence, collisional effects, and tritium/deuterium isotope selectivity", *J. Chem. Phys.*, 81, 2363-2374 (1984)

9. P. K. Gupta and S. C. Mehendale, "Mid-infrared Optically Pumped Molecular Lasers", *Hyperfine Interactions* 37, 243-274 (1987)

10. R. G. Harrison and P. K. Gupta, "Optically Pumped Mid-Infrared Molecular Gas Lasers", in Infrared and millimeter waves 7 (Academic Press, New York, 1983)

11. K. J. Siemsen, E. Williams, and J. Reid, "Alternative approach to stable lasers: the optically pumped $NH_3$ laser", *Opt. Lett.*, 12, 879-891 (1987)

12. P. Wazen and G. L. Bourdet, "CW MIR Optically Pumped Ammonia laser with Large Frequency Tunability", *Opt. Commun.* 71, 81-84 (1989)

## References


1. R. R. Jacobs, D. Prosnitz, W. K. Bischel, and C. K. Rhodes, "Laser generation from 6 to 35 $\mu$m following two-photon excitation of ammonia", *Appl. Phys. Lett.*, 29, 710-712 (1976)

2. D. F. Kroeker and J. Reid, "Line-tunable cw ortho- and para-$NH_3$ lasers operating at wavelengths of 11 to 14 $\mu$m", *Appl. Opt.*, 25, 2929-2933 (1986)

3. Handbook of Laser Science and Technology, Vol. II: Gas Lasers, ed. M.J. Weber (CRC Press, Florida, 1982)

4. B. I. Vasil'ev, A. Z. Grasyuk, A. P. Dyad'kin, A. N. Sukhanov, and A. B. Yastrebkov, "High-power efficient optically pumped $NH_3$ laser, tunable over the range 770-890 $cm^{-1}$", *Sov. J. Quantum Electron.*, 10, 64-68 (1980)

5. P. K. Gupta, A. K. Kar, M. R. Taghizadeh, and R. G. Harrison, "12.8-$\mu$m $NH_3$ laser emission with 40-60% power conversion and up to 28% energy conversion efficiency", *Appl. Phys. Lett.*, 39, 32-34 (1981)

6. R. V. Ambartsumian, A. Z. Grasiuk, A. P. Pyadkin, N. P. Furzikov, V. S. Letokhov, and B. I. Vasil'ev, "Isotopically Selective Dissociation of $CCl_4$ Molecules by $NH_3$ Laser Radiation", *Appl. Phys.*, 15, 27-30 (1978)

7. J. J. Tiee and C. Wittig, "Isotopically selective ir photodissociation of $SeF_6$", *Appl. Phys. Lett.*, 32, 236-238 (1978)

8. F. Magnotta and I. P. Herman, "Infrared laser multiple-photon dissociation of $CTCl_3$: Wavelength dependence, collisional effects, and tritium/deuterium isotope selectivity", *J. Chem. Phys.*, 81, 2363-2374 (1984)

9. P. K. Gupta and S. C. Mehendale, "Mid-infrared Optically Pumped Molecular Lasers", *Hyperfine Interactions* 37, 243-274 (1987)

10. R. G. Harrison and P. K. Gupta, "Optically Pumped Mid-Infrared Molecular Gas Lasers", in Infrared and millimeter waves 7 (Academic Press, New York, 1983)

11. K. J. Siemsen, E. Williams, and J. Reid, "Alternative approach to stable lasers: the optically pumped $NH_3$ laser", *Opt. Lett.*, 12, 879-891 (1987)

12. P. Wazen and G. L. Bourdet, "CW MIR Optically Pumped Ammonia laser with Large Frequency Tunability", *Opt. Commun.* 71, 81-84 (1989)

13. R. G. Harrison and D. J. Bisivas, "Demonstration of Self-Pulsing Instability and Transitions to Chaos in Single-Mode and Multimode Homogeneously Broadened Raman Laser", *Phys. Rev. Lett.*, 55, 63-66 (1985)

14. C. O. Weiss, W. Klische, N. B. Abraham, and U. Hubner, "Comparison of $NH_3$ Laser Dynamics with the extended Lorenz Model", *Appl. Phys. B*, 49, 211-215 (1989)

15. H. D. Morrison, Dynamics of Optically-Pumped Pulsed Mid-Infrared $NH_3$ Lasers, Ph. D. Thesis (McMaster University, Hamilton, 1985)

16. H. D. Morrison, B. K. Garside, and J. Reid, "Gain dynamics in pulsed 12-$\mu$m $NH_3$ lasers", *J. Opt. Soc. Am.* B2, 535-540 (1985)

17. H. D. Morrison , B. K. Garside, and J. Reid, "Dynamics of the Optically Pumped Midinfrared $NH_3$ Laser at High Pump Power--Part I: Inversion Gain", *IEEE J. of Quant. Electron.* QE-20, 1051-1060 (1984)

18. R. L. Sinclair, J. Reid, H. D. Morrison, B. K. Garside, and C. Rolland, "Dynamics of the line-tunable 12-$\mu$m continuous-wave $NH_3$ laser as measured with a tunable-diode laser", *J. Opt. Soc. Am.*, B2, 800-806, (1985)

19. H. Tashiro, T. Koizumi, K. Toyoda, and S. Namba, "Wide-range amplification of a tunable-diode laser using optically pumped high-pressure $NH_3$ gas", *Opt. Let.* 9, 279-281 (1984)

20. C. H. Townes and A. L. Schawlow, Microwave Spectroscopy, (Dover Publications, New York, 1975), p. 369.

21. G. Herzberg, Molecular Spectra and Molecular Structure II. Infrared and Raman Spectra of Polyatomic Molecules (Van Nostrand, New York, 1945)

22. C. Rolland, Study of Optically Pumped $NH_3$ Mid-Infrared Lasers, Masters Thesis (McMaster University, Hamilton, 1980)

23. C. Rolland, Optically-Pumped cw Mid-Infrared $NH_3$ lasers, Ph.D. Thesis (McMaster University, Hamilton, 1984)

24. P. Dubé and J. Reid, "Vibrational relaxation of the $2\nu_2$ level of $NH_3$", *J. Chem. Phys.*, 90, 2892-2899 (1989)

25. A. L. Golger and V. S. Letokhov, "Population inversion due to saturation of absorption in molecular rotation-vibrational transitions", *Sov. J. Quantum Electron.* 3, 15-20 (1973) [*Kvantovaya Elecktron.* 1, 30-40 (1973)]

26. D. J. Danagher and J. Reid, "Vibrational relaxation of the $\nu_2$=1 level of ortho and para $NH_3$", *J. Chem. Phys.*, 86, 5449-5455 (1987)

27. F. E. Hovis and C. B. Moore, "Vibrational relaxation of $NH_3(\nu_2)$", *J. Chem. Phys.*, 69, 4947-4950 (1978)

28. F. E. Hovis and C. B. Moore, "Temperature dependence of vibrational energy transfer in $NH_3$ and $H_2{}^{18}O$", *J. Chem. Phys.*, 72, 2397-2402 (1980)

29. P. H. Beckwith, D. J. Danagher, and J. Reid, "Linewidths and Linestrengths in the $\nu_2$ Band of $NH_3$ as Measured with a tunable Diode Laser", *J. Mol. Spec.*, 121, 209-217 (1987)

30. B. K. Deka, P. E. Dyer, and I. K. Perera, "High Energy Density $NH_3$ Laser using an unstable resonator $CO_2$ Laser pump", *Opt. Commun.* 32, 295-300 (1980)

31. Y. Li, K. Ichung, and H. Hsun, "A 12 $\mu$m band tunable ammonia laser", *Chinese Physics-Lasers*, 14, 66-68 (1987)

32. K. Midorikawa, K. Shimizu, H. Tashiro, and S. Namba, "High-Power, Line-Tunable $^{14}NH_3$ and $^{15}NH_3$ Lasers", *Appl. Phys. B* 38, 185-189 (1985)

33. H. Tashiro, K. Suzuki, K. Toyoda, and S. Namba, "Wide-Range Line-Tunable Oscillation of an Optically Pumped $NH_3$ Laser", *Appl. Phys.* 21, 237-240 (1980)

34. J. D. White, D. M. Bruce, P. Beckwith, and J. Reid, "Efficient optically-pumped $NH_3$ amplifiers in the 10 to 12 $\mu$m region", *Appl. Phys. B*, 50, 345-354 (1990)

35. D. M. Bruce, A. Chakrabarti, J. Reid, and J. D. White, "Efficient, optically-pumped $NH_3$ oscillators and amplifiers operating in the mid-infrared", paper presented at the CLEO Conference, Anaheim, 1988.

36. M. Akhrarov, B. I. Vasil'ev, A. Z. Grasyuk, and V. I Soskov, "Ammonia laser pumped transversely by optical radiation", *Sov. J. Quantum Electron.* 16, 453-455 (1986)

37. H. D. Morrison, B. K. Garside, and J. Reid, "Modeling of High-Pressure 12-$\mu$m $NH_3$ Lasers", *Appl. Phys. B*, 37, 165-170 (1985)

38. P. B. Corkum, "Amplification of picosecond 10 $\mu$m pulses in Multiatmosphere $CO_2$ Lasers," *IEEE. J. Quantum Electron.*, QE-21, 216-232 (1985)

39. K. Stenersen and G. Wang, "New Direct Optical Pump Schemes for Multiatmosphere $CO_2$ and $N_2O$ Lasers", *IEEE J. Quantum Electron.*, QE-25, 147-153 (1989)

40. F. W. Taylor, "Spectral Data For the $\nu_2$ bands of Ammonia with Applications to radiative Transfer in the Atmosphere of Jupiter", *J. Quant. Spectrosc. Radiat. Transfer* 13, 1181-1217 (1973)

41. A. N. Bobo'rovskii, A. A. Vedenov, A. V. Kozhevnikov, and D. N. Sobolenko, "$NH_3$ laser pumped by two $CO_2$ lasers", *JETP Lett.*, 29, 536-539 (1979)

42. P. Pinson, A. Delage, G. Girard, and M. Michon, "Characteristics of two-step and two-photon-excited emissions in $^{14}NH_3$", *J. Appl. Phys.*, 52, 2634-2637 (1981)

43. H. D. Morrison, J. Reid, B. K. Garside, "16-21-$\mu$m line-tunable $NH_3$ laser produced by two-step optical pumping", *Appl. Phys. Lett.* 45, 321-323 (1984)

44. P. Dubé, Collisional Energy Transfer From the $2\nu_2$ Level of $NH_3$ Measured With a Tunable Diode Laser, Masters Thesis (McMaster University, Hamilton, 1988)

45. S. Urban, V. Spirko, D. Papousek, R. S. McDowell, N. G. Nereson, S. P. Belov, L. I. Gershstein, A. V. Maslovsky, A. F. Rupnov, J. Curtis, and K. N. Rao, "Coriolis and $l$-Type Interactions in the $\nu_2$, $2\nu_2$, and $\nu_4$ States of $^{14}NH_3$", *J. Mol. Spec.* 79, 455-495 (1980)